Ventral motor thalamic input to prelimbic cortex, but not to striatum, mediates cost-benefit decision-making in rats

Bianca Sieveritz*,[1] Shannon Hayashi Duke[1], Jeffery R. Wickens[1] and Gordon W. Arbuthnott[1]

[1]Okinawa Institute of Science and Technology Graduate University, 1919-1 Tancha, Onna-son, Okinawa, 904-0495 Japan

Abstract

Both prelimbic corticostriatal neurons and striatal fast-spiking interneurons contribute to decisions that require a trade-off between cost and benefit. We investigated whether ventral motor thalamic input to prelimbic cortex or striatum contributes to cost-benefit decision-making. Optogenetic inhibition of ventral motor thalamic axon terminals in prelimbic cortex biased rats towards a high cost-high benefit option and, in anesthetized rats, decreased neuronal activity in deep layers of prelimbic cortex. Stimulation of ventral motor thalamic nuclei induced a neuronal response in deep layers of prelimbic cortex and simultaneous optogenetic inhibition of layer 1 inhibitory interneurons similarly decreased neuronal activity. Chemogenetic inhibition of striatal-projecting ventral motor thalamic neurons did not affect cost-benefit decision-making. Our results indicate that ventral motor thalamic input to prelimbic cortex, but not striatum, mediates cost-benefit decision-making, probably by regulating prelimbic corticostriatal neuron activity directly as well as indirectly through a network of cortical inhibitory interneurons.

Keywords: ventral motor thalamus; prelimbic cortex; striatum; cost-benefit decision-making; approach-avoidance; layer 1 inhibitory interneurons; corticostriatal neurons; optogenetics

Introduction

Prefrontal cortical areas are involved in a variety of decisions that require a trade-off: Anterior cingulate cortex regulates the willingness to expend physical (Walton et al., 2003) or mental effort to receive a larger reward (Hosking et al., 2014), orbitofrontal cortex is necessary in risk- and delay-based decision-making (Mobini et al., 2002), dorsomedial prefrontal corticostriatal neurons encode approach-avoidance behavior (Loewke et al., 2021), and prelimbic corticostriatal neurons mediate the trade-off between a more costly, more beneficial and a less costly, less beneficial option (Friedman et al., 2015). Recent studies have highlighted the importance of rodent ventral motor thalamic nuclei (ventromedial, ventral anterior and ventrolateral thalamic nucleus; MT) in tasks that require animals to choose between two options (Catanese and Jaeger, 2021; Gaidica et al., 2018; Guo et al., 2017). In rodents, MT sends dense projections to prelimbic cortex (Arbuthnott et al., 1990; Herkenham, 1979) and some MT neurons send collaterals to striatum (Elena Erro et al., 2002; Kuramoto et al., 2009), raising the question whether MT input to prelimbic cortex or striatum is involved in decisions that require a trade-off.

A previous study has shown that optogenetic inhibition of prelimbic corticostriatal neurons biased rats towards a more costly, more beneficial option (Friedman et al., 2015). In contrast, the same perturbation did not affect choices made between a high and low benefit, or a high and low cost option (Friedman et al., 2015). We and others previously showed that MT projections to prelimbic cortex preferentially contact corticostriatal pyramidal neurons (Arbuthnott et al., 1990; Collins et al., 2018; Sieveritz and Arbuthnott, 2020). Hence, our first experiment investigated whether MT input to prelimbic cortex is necessary in cost-benefit decision-making. We demonstrated that optogenetic inhibition of MT axon terminals in prelimbic cortex biased rats towards a high cost-high benefit option.

(Friedman et al., 2015) further showed that optogenetic inhibition of prelimbic corticostriatal neurons in cost-benefit decision-making also disinhibited striatal fast-spiking interneurons. Involvement of striatum in cost-benefit decision-making was also confirmed in macaques (Amemori et al., 2020). Like prelimbic cortex, striatum receives input from MT. Some MT neurons that project to cortex send collaterals to striatum (Elena Erro et al., 2002; Kuramoto et al., 2009). We will refer to them as MT striatal-projecting neurons. Striatal-projecting neurons that originate in MT and other midline/intralaminar thalamic nuclei target striatal inhibitory interneurons (Johansson and Silberberg, 2020; Klug et al., 2018; Sidibé and Smith, 1999; Smith et al., 2004) and striatal fast-spiking interneurons (Johansson and Silberberg, 2020; Klug et al., 2018; Nakano et al., 2018); the very same striatal interneurons that are disinhibited by optogenetic inhibition of prelimbic corticostriatal neurons in cost-benefit decision-making (Friedman et al., 2015). Hence, our second experiment investigated whether MT striatal-projecting neurons are necessary in cost-benefit decision-making.

Our third and fourth experiment investigated a potential mechanism to explain how optogenetic inhibition of MT input to prelimbic cortex might induce the observed bias in cost-benefit decision-making. MT provides input to prelimbic pyramidal neurons and prelimbic layer 1 inhibitory interneurons (Collins et al., 2018; Sieveritz and Arbuthnott, 2020). Layer 1 inhibitory interneurons, in turn, inhibit a network of cortical inhibitory interneurons (Cruikshank et al., 2012), which regulates the activity of deep layer pyramidal neurons (Jiang et al., 2013; Lee et al., 2015). Given our results we propose that MT input to both prelimbic pyramidal neurons and prelimbic layer 1 inhibitory interneurons is necessary to regulate the activity of corticostriatal pyramidal neurons in prelimbic cortex. We further propose that inhibition of MT input reduces the activity of these corticostriatal pyramidal neurons and induces the observed behavioral bias.

Results

We trained 4- to 7-week-old male Sprague-Dawley rats on a benefit-benefit, cost-cost and cost-benefit decision-making task. Rats were presented with two retractable levers and each lever was associated with a specific combination of benefit and cost (Figure 1A). On the benefit-benefit decision-making task one lever was associated with a high benefit paired with a low cost, and the other lever was associated with a low benefit paired with a low cost. On the cost-cost decision-making task one lever was associated with a high cost paired with a high benefit, while the other lever was associated with a low cost paired with a high benefit. On the cost-benefit decision-making task one lever was associated with a high cost paired with a high benefit, while the other lever was associated with a low cost paired with a low benefit. The high benefit in all tasks was 0.1 mL of sweetened condensed milk diluted at 20% and the low benefit was 0.1 mL of sweetened condensed milk that had been further diluted than the high reward (1-19%) or tap water. The high cost was a bright light presented at 1.75 kLx for 10 secs, and the low cost was a dim light presented at 1.0 lx for 10 secs. The first three days of behavioral training on the cost-benefit decision-making task were used to adjust the dilution of the sweetened condensed milk delivered as the low benefit, so that rats would choose both the high cost-high benefit and the low cost-low benefit option in about 50% of the trials.

Optogenetic inhibition of MT input to prelimbic cortex biased rats towards a high cost-high benefit option

At 9 weeks of age, twenty-two rats that had learned all three decision-making tasks received unilateral virus injections into MT. We injected 50-70 nl of either an adeno-associated virus expressing archaerhodopsin (AAV5-CAG-ArchT-GFP, n=10; ArchT rats) or a control virus (AAV5-CAG-GFP, n=12; controls). In addition, we implanted a short optical fiber attached

to a 590 nm light emitting diode (LED fiber optic) through the contralateral hemisphere into ipsilateral prelimbic cortical layer 1 (Figure 1B). We confirmed that virus injections were primarily confined to MT (Figure 1C). Tips of LED fiber optics were located in prelimbic cortical layer 1 in close proximity to virus-expressing MT axon terminals (Figure 1C).

After a 12- to 16-day-long recovery period, we assessed rats' choice behavior. For each of the three decision-making tasks, rats were presented with 40 trials per day on 3 consecutive days. We compared rats' choice behavior without (light OFF) and with delivery of the 590 nm light (light ON). In ArchT rats, delivery of the 590 nm light induced optogenetic inhibition of virus-expressing MT axon terminals in prelimbic cortical layer 1. On each day, the first 20 trials were light OFF trials, while the last 20 trials were light ON trials. Optogenetic inhibition of MT axon terminals in prelimbic cortical layer 1 on the cost-benefit decision-making task biased rats towards the high cost-high benefit option (Figure 1D). In contrast, choice behavior on the benefit-benefit and cost-cost decision-making tasks was not affected (Figure 1E and 1F). To compare the percentage of high cost-high benefit choices on the cost-benefit decision-making task, we performed a mixed-design ANOVA with the injected virus as between animal factor and light ON/OFF as within animal factor. We observed a significant interaction effect between the injected virus and light ON/OFF ($p=0.031$, Cohen's $F=0.517$, $df=1$). and a main effect for light ON/OFF ($p=0.005$, Cohen's $F=0.707$, $df=1$). We performed post-hoc testing using multiple t-tests and applied a Bonferroni correction to account for multiple comparisons (adjusted significance level=0.0028). In light ON trials, we observed a significant increase in the percentage of high cost-high benefit choices for ArchT rats ($p=0.00004$, $r=0.926$, $df=9$), but not for controls ($p=0.552$, $r=0.182$, $df=11$). This indicates that optogenetic inhibition of MT axon terminals in prelimbic layer 1 biased rats' choices towards the high cost-high benefit option (Figure 1D). To determine whether the

126 increase in the percentage of high cost-high benefit choices from light OFF to light ON trials
127 differed significantly between controls and ArchT rats, we used an uncorrected Student's t-
128 test. The increase was significantly larger for ArchT rats than for controls ($p=0.026$, $r=0.536$,
129 $df=20$), further confirming that optogenetic inhibition of MT input to prelimbic cortex biased
130 choices towards the high cost-high benefit option.
131
132 Although not significant, we observed a similar trend when data was split by day (Figure 1 -
133 figure supplement 1). Given that only 20 light ON and OFF trials were administered on each
134 individual day of behavioral testing, it is not surprising that none of the effects reached
135 significance on any individual day. However, we did observe an increase in high-cost high-
136 benefit choices in ArchT rats in light ON trials on the second day of behavioral testing that
137 approached significance ($p=0.0037$, $r=0.791$, $df=9$; adjusted significance level=0.0028).
138

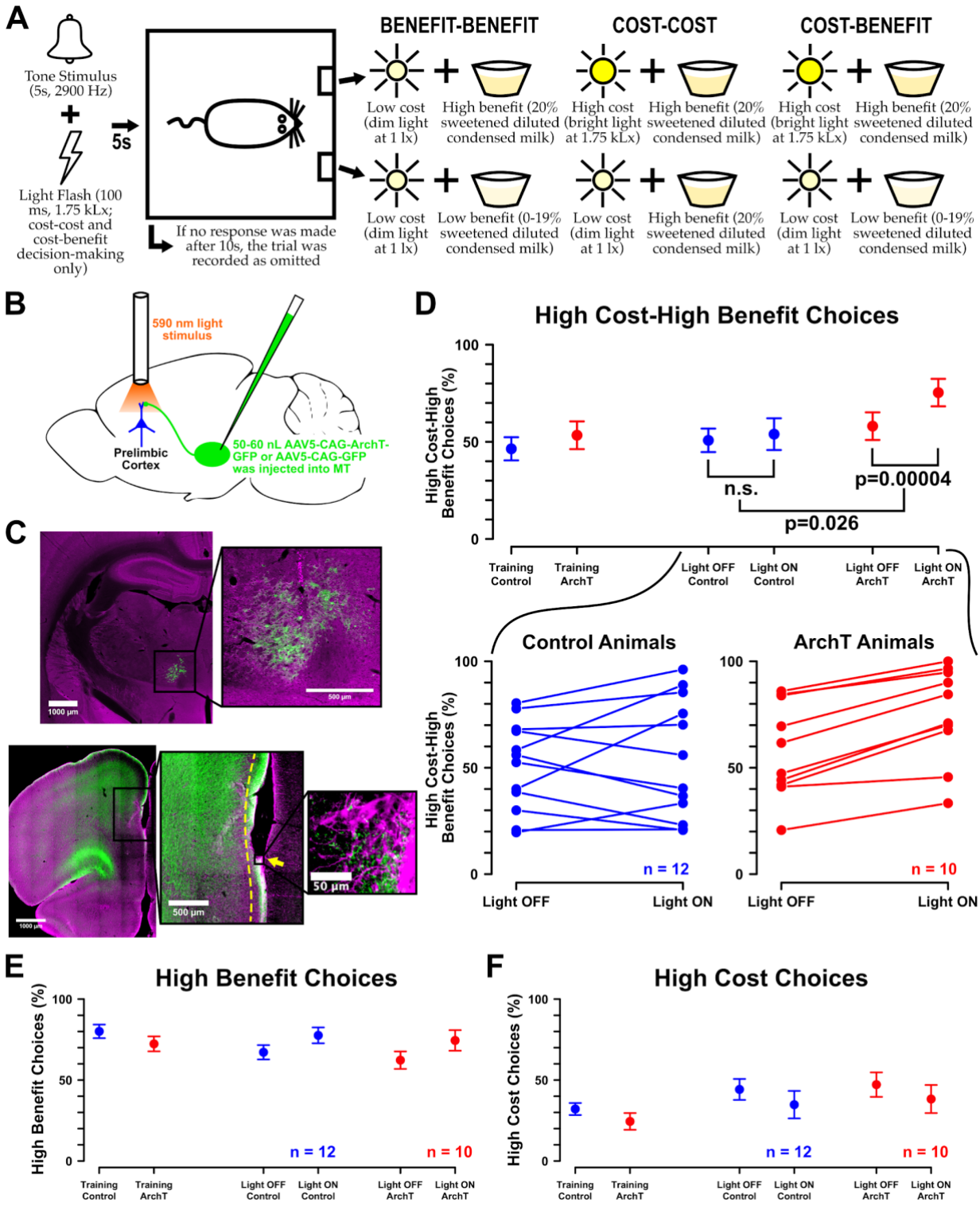

Figure 1. Optogenetic inhibition of MT axon terminals in prelimbic cortical layer 1 biases rats towards a high cost-high benefit option A- Illustration of the sequence of events on each trial. B- 50-70 nL of either AAV5-CAG-ArchT-GFP or the control virus AAV5-CAG-GFP were injected unilateral into MT and an LED fiber optic was implanted into ipsilateral

144 prelimbic cortical layer 1. C- Upper illustration: Virus expression (green) was confined to
145 MT, which was counterstained with GAD67 (magenta). Lower illustration: Virus-expressing
146 MT axon terminals (green) and the LED fiber optic tip (yellow arrow) were located in
147 prelimbic cortical layer 1. The yellow dashed line marks the approximate span of prelimbic
148 cortical layer 1. Glial fibrillary acid protein, a neuronal marker for gliosis, is marked in
149 magenta. D- Upper illustration: Mean percentage of high cost-high benefit choices +/- the
150 standard error of the mean for controls (blue) and ArchT rats (red). For behavioral training,
151 the mean across the first 20 trials on the last day of training is shown. For behavioral testing,
152 data are separated between light ON and OFF trials. Lower illustration: Mean percentage of
153 high cost-high benefit choices in light ON and OFF trials for each individual control (blue)
154 and ArchT rat (red). E- Mean percentage of high benefit and F- high cost choices +/- the
155 standard error of the mean for controls (blue) and ArchT rats (red).
156

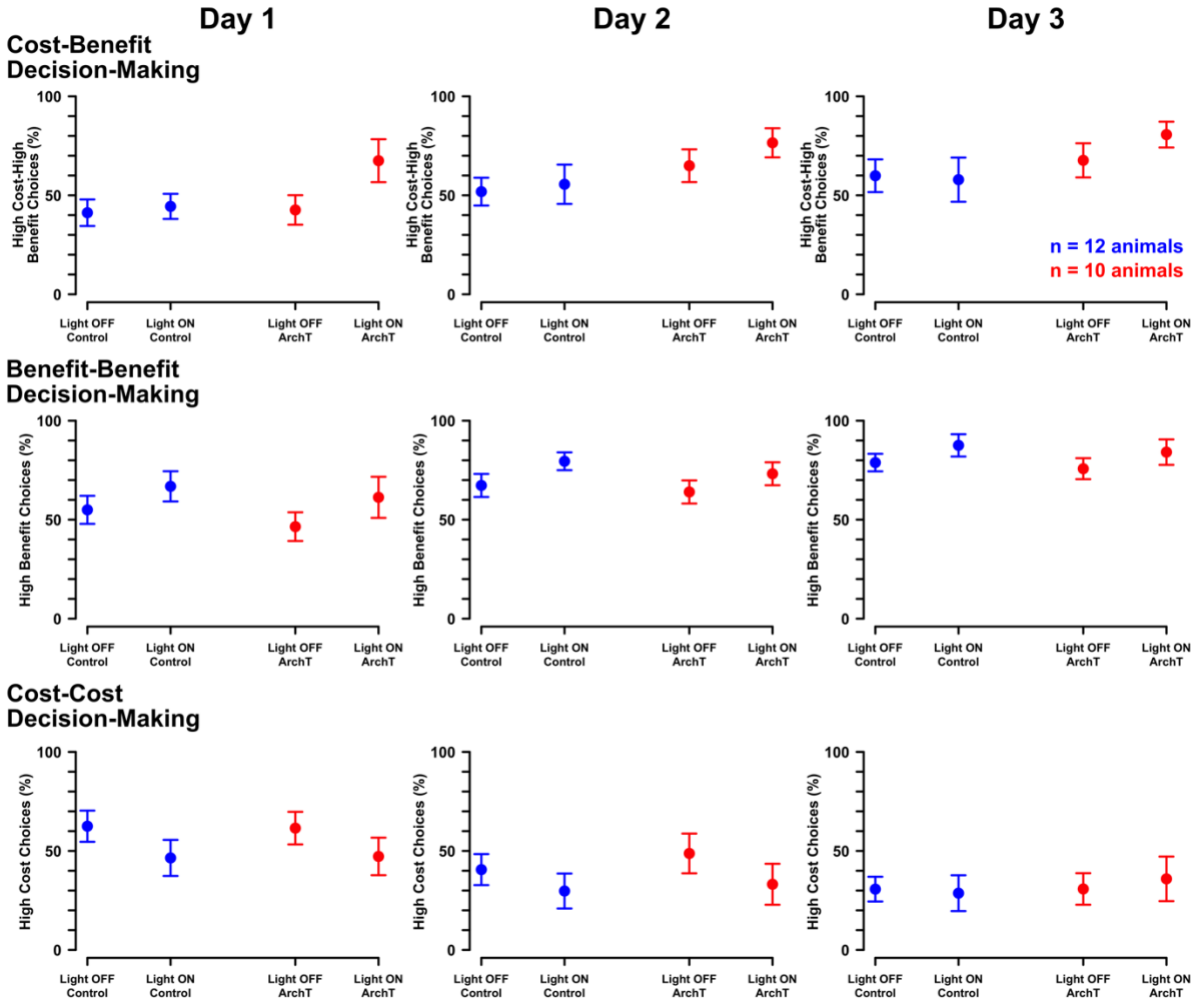

Figure 1 – figure supplemental 1. Data split by individual behavioral testing days showed similar trends to data averaged across all behavioral testing days. Mean percentage of high cost-high benefit, high benefit or high cost choices +/- standard error of the mean for controls (blue) and ArchT rats (red) in light ON and OFF trials on each individual day of behavioral testing.

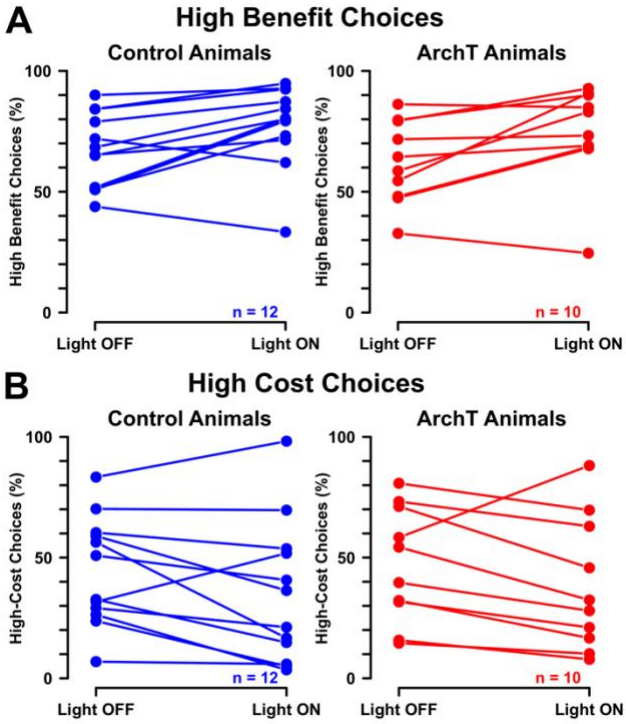

Figure 1 – figure supplemental 2. Data on the benefit-benefit and cost-cost decision-making task for each individual animal. A- Mean percentage of high benefit and B- high cost choices for each individual controls (blue) and ArchT rat (red) in light ON and OFF trials.

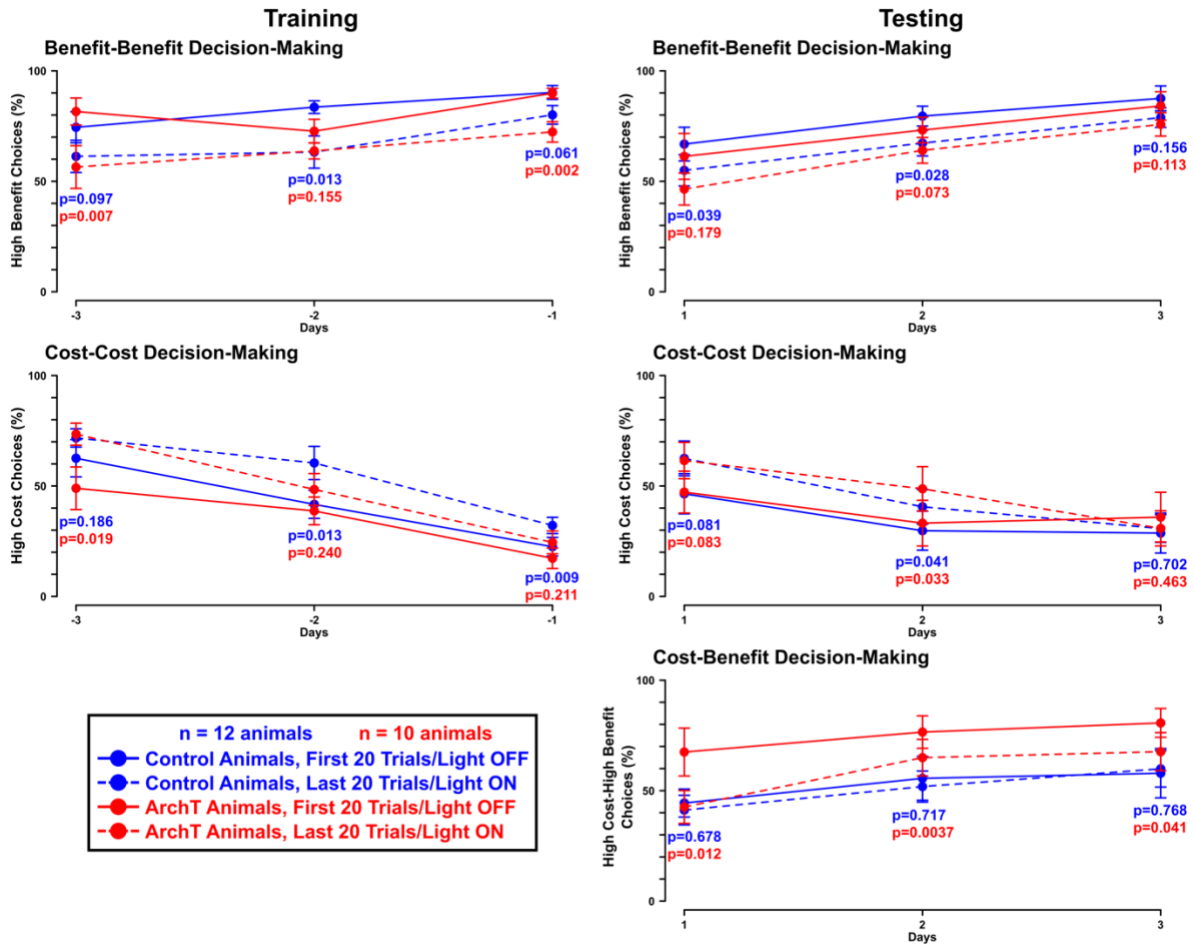

Figure 1 – figure supplemental 3. Rats show a within session retention effect on the benefit-benefit and cost-cost decision-making task. We compared the choice behavior on the first and last 20 trials on the last three days of behavioral training and on each day of behavioral testing. Plots show the mean percentage of high benefit, high cost or high cost-high benefit choices +/- the standard error of the mean for controls (blue) and ArchT rats (red) on the first or last 20 trials on each day on the last three days of behavioral training and on each day of behavioral testing. For behavioral testing the first 20 trials were light OFF trials, while the last 20 trials were light ON trials. Data on the percentage of high cost-high benefit choices is not presented for the last three days of behavioral training, since the first three days of training were used to titrate the dilution of sweetened condensed milk for each rat. Data that includes the first three training days, which is the case for most rats, does not represent the

181 actual choice behavior of rats after titration of the sweetened condensed milk dilution. Effects
182 sizes are indicated in Appendix 1 – Table 1.
183

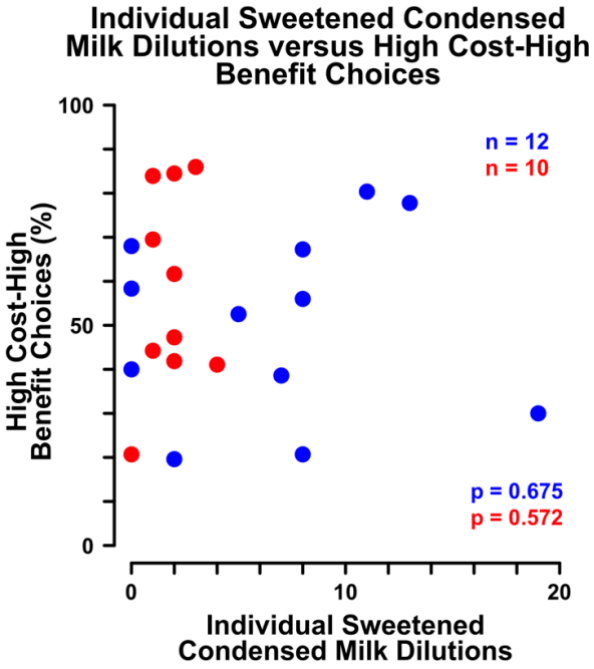

184
185 Figure 1 - figure supplement 4. Correlation between individual dilution of sweetened
186 condensed milk determined for each rat and high cost-high benefit choices for controls (blue)
187 and ArchT rats (red).
188

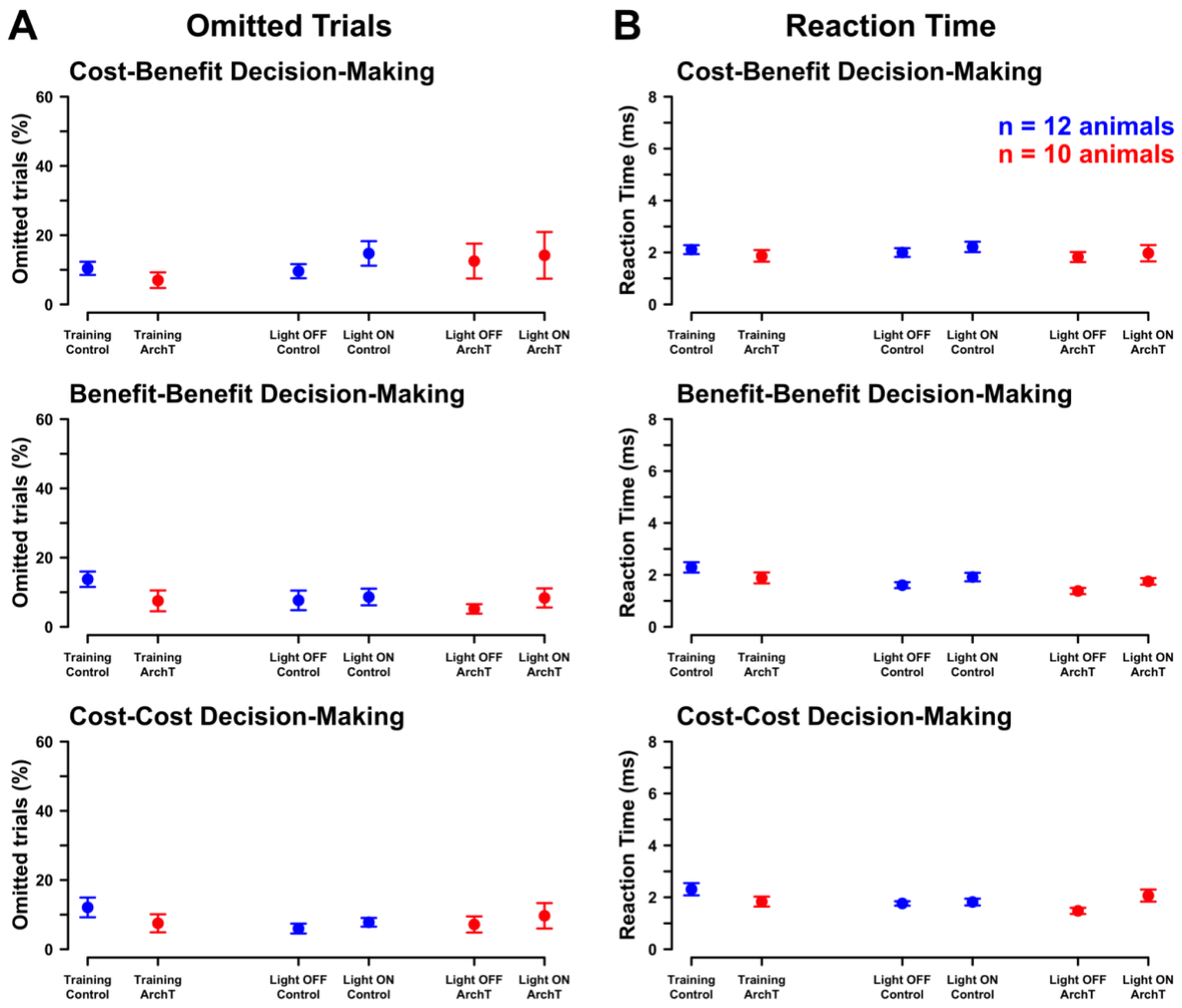

Figure 1 – figure supplemental 5. Percentage of omitted trials and reaction times on non-omitted trials upon optogenetic inhibition of MT axon terminals in prelimbic cortical layer 1. Plots show the mean percentage of omitted trials or reaction times on non-omitted trials +/- the standard error of the mean on the cost-benefit, benefit-benefit and cost-cost decision-making task for controls (blue) and ArchT rats (red) averaged over the first 20 trials on the last day of behavioral training, in light ON and OFF trials.

No changes in choice behavior were observed on the benefit-benefit and cost-cost decision-making tasks

We observed a main effect of light ON/OFF in the benefit-benefit ($p=0.001$, Cohen's $F=0.903$, $df=1$) and cost-cost decision-making tasks ($p=0.014$, Cohen's $F=0.605$, $df=1$).

However, post-hoc testing (Bonferroni correction applied to account for multiple comparisons; adjusted significance level=0.0028) did not confirm that the percentage of high benefit choices (ArchT: p=0.019, r=0.690, df=9; controls: p=0.016, r=652, df=11; Figure 1E and Figure 1 - figure supplement 2A) or high cost choices (ArchT: p=0.093, r=0.531, df=9; controls: p=0.076, r=0.508, df=11; Figure 1F and Figure 1 - figure supplement 2B) had changed significantly. This indicates that optogenetic inhibition of MT terminals in prelimbic cortex did not alter choice behavior in either of these two tasks.

Given that we used a block design and observed an increase in the percentage of high benefit choices and a decrease in the percentage of high cost choices from the first to the second half of each behavioral training session (Figure 1 – figure supplement 3), it is likely that the main effect of light ON/OFF was caused by a within session retention effect. However, the observed effect might instead have been due to unexpected electrophysiological side effects caused by exposure of the brain tissue to the 590 nm light, which was delivered to prelimbic cortical layer 1 in light ON trials. When we plotted the percentage of high benefit or high cost choices on the first and last 20 trials on the last 3 days of behavioral training (Figure 1 – figure supplement 3), we observed an increase of high benefit and a decrease of high cost choices between the first and last 20 trials on each of the last 3 days of behavioral training (Figure 1 – figure supplement 3). Given that we observed this effect during behavioral training, which happened prior to implantation of the 590 nm LED fiber optics, a within session retention effect is a more likely explanation than a side effect of the 590 nm light. In our experiments, the 590 nm light was delivered at a maximum intensity of 1.2mW and for a maximum of 20 secs in our experiments. In brain slices, delivery of a 532 nm light stimulus at 1 mW for up to 30 secs did not change the firing rate of cortical neurons (Stujenske et al., 2015), making it unlikely that light delivery alone increased or decreased neuronal activity.

Moreover, given the numerical aperture and core radius of our optical fibers, a 561 nm light stimulus delivered at 1.2 mW is reduced to as little as 0.14 mW/mm2 at a 1 mm distance from the fiber tip (Deisseroth, 2021), making it even less likely that light delivery caused unexpected side effects in our experiments.

Effects are not explained by pre-existing differences in choice behavior or caused by surgery

We confirmed that none of the behavioral effects, or the absence thereof, were explained by pre-existing differences in choice behavior. Choice behavior of controls and ArchT rats was comparable before and in light OFF trials after the surgery ($p>0.0028$; Figure 1D, 1E and 1F; for detailed p-values and effect sizes see Appendix 1 - Table 2). We further confirmed that behavioral effects or the absence thereof were not caused by surgery. No significant changes in choice behavior were observed pre- as compared to post-surgery for either controls or ArchT rats ($p>0.0028$; Figure 1D, 1E and 1F; for detailed p-values and effects sizes see Appendix 1 - Table 2). Lastly, we confirmed that reward sensitivity in light OFF trials as indicated by individually determined sweetened condensed milk dilutions did not correlate with the percentage of high cost-high benefit choices (Figure 1 - figure supplemental 4; ArchT: Kendall's Tau=0.149, p=0.572, df=9; controls: Kendall's Tau=0.095, p=0.675, df=11).

Optogenetic inhibition of MT axon terminals in prelimbic cortex did not disrupt motor function

Given that we inhibited axon terminals emerging from MT, a brain region known to be heavily involved in motor control, we might have interfered with the rats' motor function. To confirm that motor function was not disrupted, we compared the percentage of omitted trials as well as the average reaction time on non-omitted trials between light ON and OFF trials

within ArchT rats and within controls (Figure 1 – figure supplement 5). Comparing the percentage of omitted trials, we observed a main effect for light ON/OFF on the cost-benefit decision-making task ($p=0.035$, Cohen's $F=0.506$, $df=1$). Comparing the average reaction time, we observed an interaction effect ($p=0.025$, Cohen's $F=0.542$, $df=1$) and a main effect for light ON/OFF on the cost-cost ($p=0.013$, Cohen's $F=0.607$, $df=1$) as well as a main effect for light ON/OFF on the benefit-benefit decision-making task ($p=0.001$, Cohen's $F=0.855$, $df=1$). However, post-hoc testing with an applied Bonferroni correction for multiple comparisons (adjusted significance level=0.0083) did not confirm any of these effects ($p>0.0083$, for detailed p-values and effect sizes see Appendix 1 - Table 2). Hence, we concluded that our rats' motor function was not disrupted. Rats were able to move towards the lever and to move at comparable speeds in light ON and OFF trials.

Chemogenetic inhibition of MT striatal-projecting neurons did not induce a bias on the cost-benefit decision-making task

Midline and intralaminar thalamic nuclei provide input to striatal fast-spiking interneurons (Johansson and Silberberg, 2020; Klug et al., 2018; Nakano et al., 2018); the same neurons that show altered activity in cost-benefit decision-making during optogenetic stimulation or inhibition of prelimbic corticostriatal neurons (Friedman et al., 2015). Hence, we explored whether chemogenetic inhibition of MT striatal-projecting neurons also induces a bias in choice behavior on the cost-benefit decision-making task. However, we first verified that MT thalamostriatal projection neurons project to striatal fast-spiking interneurons in striatum. Given that midline and intralaminar thalamostriatal projection neurons also provide input to plateau-depolarization low-threshold spike neurons (PLTS neurons; Sidibé and Smith, 1999; Smith et al., 2004) and cholinergic interneurons (Johansson and Silberberg, 2020; Klug et al.,

2018; Lapper and Bolam, 1992), we further tested whether MT striatal-projecting neurons also project to these two types of neurons.

To definitively label MT striatal-projecting neurons, we used a method called retro-DREADDs (Augur et al., 2016), which allowed us to express an adeno-associated virus tagged with hM4Di and a fluorochrome in specific projection neurons. First, we injected 50-60 nL of either a Cre-dependent virus tagged with hM4Di and mCherry (AAV5-hSyn-DIO-hM4D(Gi)-mCherry, n=13) or a control virus without the hM4Di tag (AAV5-hSyn-DIO-mCherry, n=11) into MT. In the same surgery, we injected 300 nL of a retrograde, Cre-expressing adeno-associated virus into striatum (AAVrg-pmSyn1-EBFP-Cre; Figure 2A). The approach resulted in specific labeling of MT striatal-projecting neurons (Figure 2B). Labeled terminals of these MT neurons in striatum were found in close proximity to fast-spiking interneurons stained for parvalbumin (Tepper et al., 2018) (PV), PLTS neurons stained for brain nitric oxide synthase (Tepper et al., 2018) (bNOS) and cholinergic interneurons stained for choline acetyltransferase (Tepper et al., 2018) (CHAT; Figure 2C). Thus, it is likely that MT striatal-projecting neurons provide input to fast-spiking interneurons, PLTS neurons and cholinergic interneurons in striatum.

The injected animals, a total of twenty-four male Sprague-Dawley rats, had all successfully learned the three decision-making tasks described above. We tested whether chemogenetic inhibition of MT striatal-projecting neurons biased rats on any of the three decision-making tasks. We compared the choice behavior of rats that had been injected with the hM4Di-tagged virus and expressed hM4Di in MT striatal-projecting neurons (hM4Di rats) with the choice behavior of controls. We compared the choice behavior after an intraperitoneal injection of either D21 agonist or saline. In hM4Di rats, the D21 agonist activates the hM4Di receptors

expressed in MT striatal-projecting neurons, which chemogenetically inhibits the neurons. In controls, the D21 agonist does not affect neuronal activity.

For each decision-making task rats were presented with 60 trials per day on two consecutive days. Saline was injected on one of the days and D21 agonist on the other day. To our surprise, inhibition of MT striatal-projecting neurons upon injection of the D21 agonist did not induce behavioral changes in either group of rats (Figure 2D, 2E and 2F). The absence of effects cannot be explained by pre-existing differences in choice behavior between controls and hM4Di rats (Figure 2D, 2E and 2F). Furthermore, the absence of effects was not caused by surgery. The choice behavior within each group of rats was comparable pre- and post-surgery (Figure 2D, 2E and 2F).

Chemogenetic inhibition did not disrupt motor function. We compared the percentage of omitted trials as well as the average reaction time on non-omitted trials between between D21 agonist and saline trials within hM4Di rats and within controls. An ANOVA showed no main or interaction effects ($p>0.05$). hM4Di rats were able to move towards the lever after D21 agonist injections and moved towards it at a comparable speed (Figure 2 - figure supplement 1).

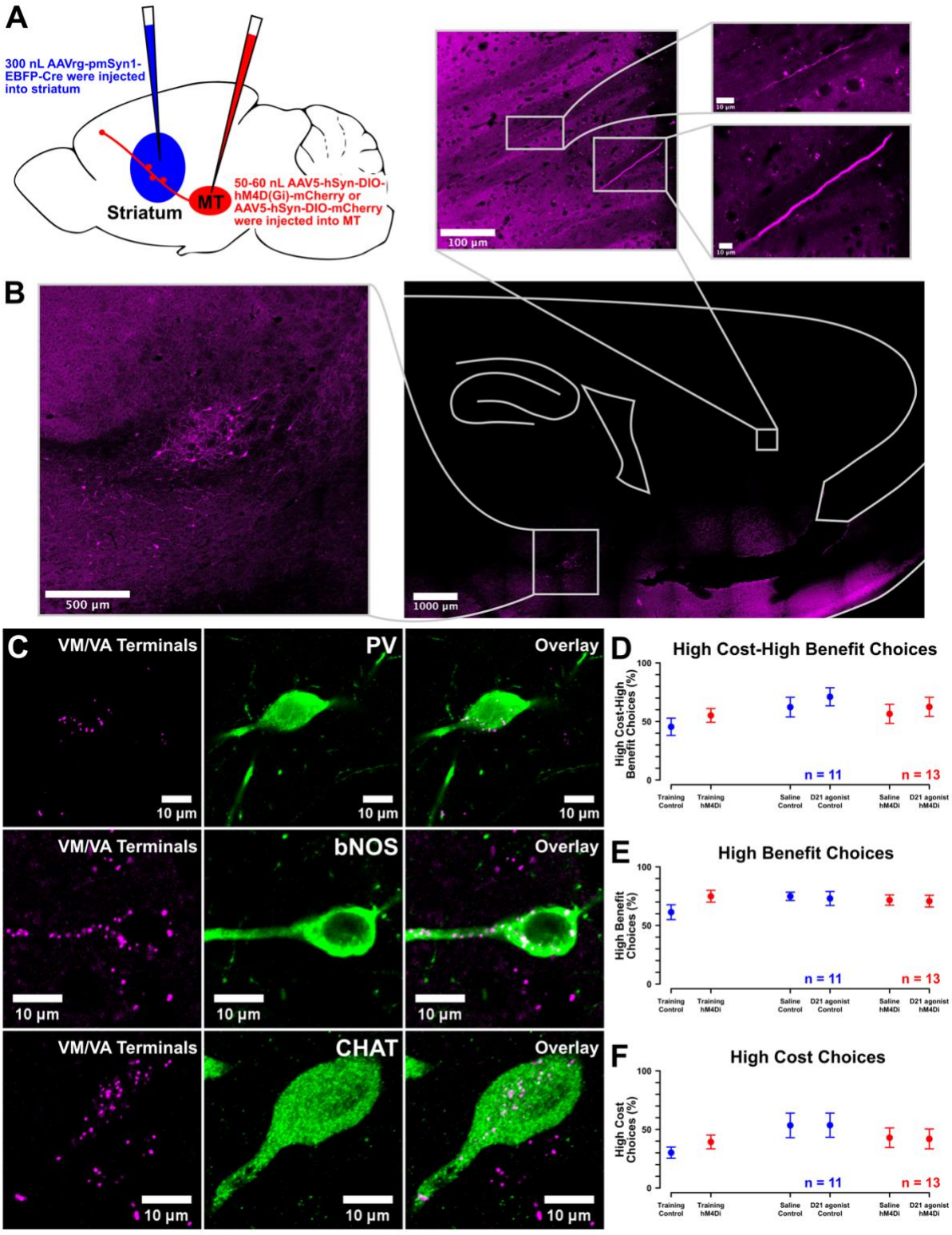

Figure 2. Chemogenetic inhibition of MT striatal-projecting neurons did not induce a bias on the cost-benefit, benefit-benefit or cost-cost decision-making task. A- 50-60 nL of either AAV5-hSyn-DIO-hM4D(Gi)-mCherry or the control virus AAV5-hSyn-DIO-mCherry were injected into MT. In the same surgery, 300 nL AAVrg-pmSyn1-EBFP-Cre were injected into

striatum. B- The left illustration shows that virus expression in neurons as classified by the spread of mCherry (magenta) was primarily confined to MT. The illustration on the top shows that virus was expressed in MT axons in striatum (magenta). C- MT axons in striatum target striatal cell bodies of PV-, bNOS- and CHAT-expressing interneurons. D- Mean percentage of high cost-high benefit, high benefit or high cost choices +/- standard error of the mean of controls (blue) and hM4Di rats (red) across the first 20 trials on the last day of behavioral training, across the 60 trials after saline injection, or across the 60 trials after D21 agonist injection (0.1 mg/kg).

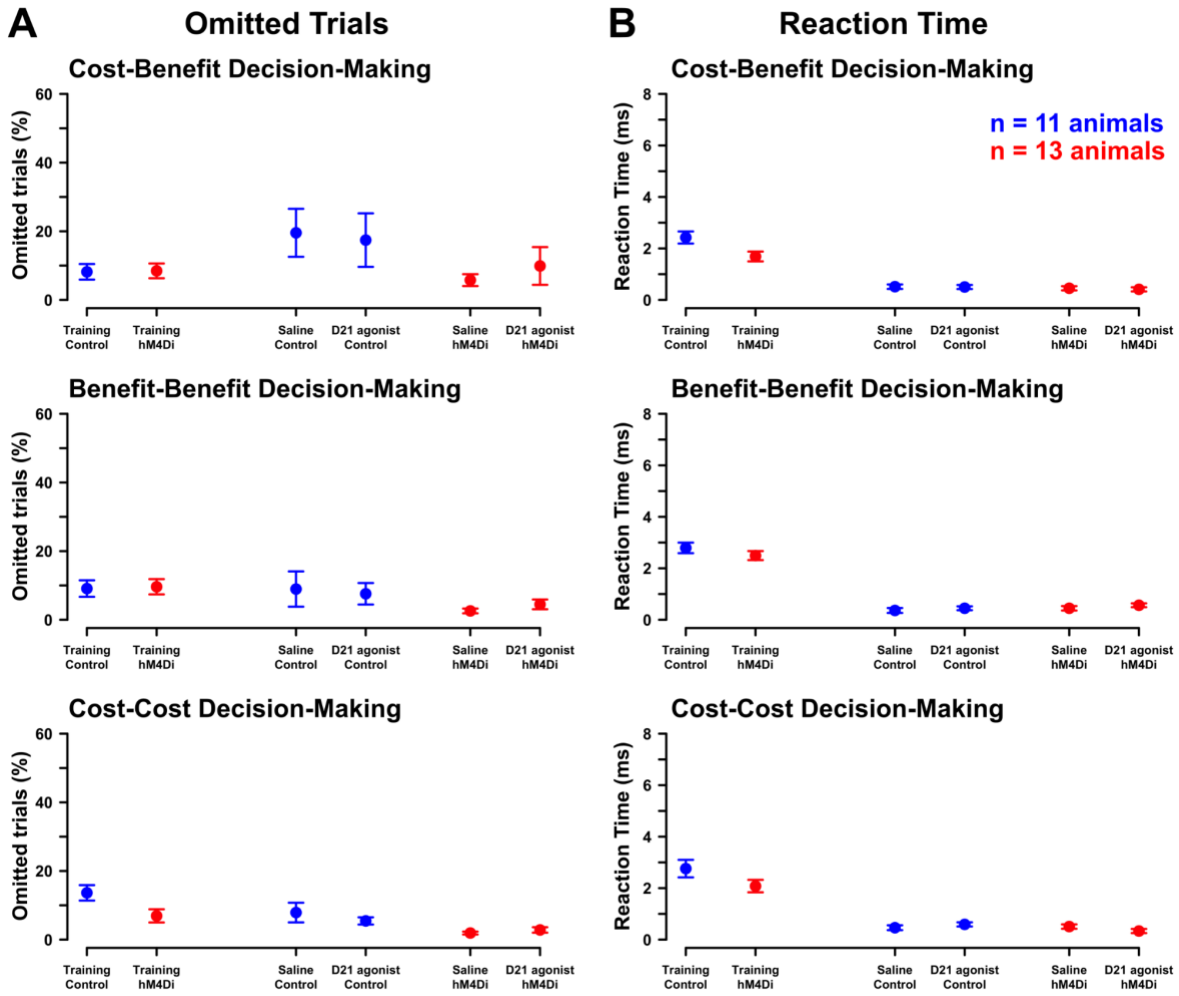

Figure 2 - figure supplemental 1. Percentage of omitted trials and reaction times upon chemogenetic inhibition of MT striatal-projecting neurons. Plots show the mean percentage

of omitted trials or reaction times on non-omitted trials +/- the standard error of the mean on the cost-benefit, benefit-benefit and cost-cost decision-making task for controls (blue) and hM4Di rats (red) averaged over the first 20 trials of the last day of behavioral training, on saline and on D21 agonist trials.

Optogenetic inhibition of MT input to prelimbic cortex decreases the activity of deep layer pyramidal neurons

We explored a possible mechanism that explains how MT input to prelimbic cortex regulates cost-benefit decision-making. In accordance with our first behavioral experiment, unilateral injections of 50-70 nl AAV5-CAG-ArchT-GFP were placed in MT in four 9- to 11-week-old male Sprague-Dawley rats. After a 12- to 16-day-long recovery period, rats were prepared for *in vivo* recording experiments under isoflurane anesthesia. An optical fiber, which was coupled to a 590 nm LED, was inserted through the contralateral hemisphere and placed in ipsilateral prelimbic cortical layer 1. To stimulate MT, a bipolar stimulating electrode was placed in ipsilateral MT. A glass electrode filled with 3.0M potassium methyl sulfate ($KMeSO_4$) and goat anti-rat Alexa Fluor 594 (dilution between 1:50 to 1:200) was lowered into deep layers of ipsilateral prelimbic cortex to record extracellular neuronal activity (Figure 3A). Virus injection sites were comparable to the one presented in Figure 1B. Figure 3B and 3D illustrate the placement of optical fibers, bipolar stimulating electrodes and glass recording electrodes.

While we recorded extracellular neuronal activity from neuronal clusters in deep layers of prelimbic cortex, we stimulated MT nuclei for 0.5 ms at -5 mA to induce a response in the recorded neuronal clusters (light OFF). Figure 3C shows an example of evoked spikes and of recorded spontaneous activity. When MT stimulation evoked a response, we simultaneously

delivered 590 nm light to prelimbic cortical layer 1 to optogenetically inhibit MT axon terminals (light ON). Simultaneous optogenetic inhibition of MT input to prelimbic cortex did not completely silence the activity of neuronal clusters in deep layers of prelimbic cortex. However, the average number of extracellular spikes per millisecond observed between 2 and 20 ms after MT stimulation significantly decreased from an average of 0.11 spikes per millisecond without optogenetic inhibition to 0.06 spikes per millisecond under optogenetic inhibition (paired t-test, p=6.6e-8, df=38, Figure 3E). Our results indicate that MT input to neurons in deep layers of prelimbic cortex can evoke a response in these neurons. Optogenetic inhibition of MT input decreases the number of induced extracellular spikes. We propose that optogenetic inhibition of MT axon terminals in prelimbic layer 1 reduces the activity of corticostriatal pyramidal neurons in prelimbic cortex and, in turn, causes the observed behavioral bias towards a high cost-high benefit option.

Observed spikes are wider after MT stimulation than during segments of spontaneous activity (Figure 3G and 3H) and are widest when MT stimulation is paired with optogenetic inhibition of MT axon terminals in prelimbic cortical layer 1 (Figure 3I). Calcium-dependent spikes in cortex are wider (De La Peña and Geijo-Barrientos, 2000; Pockberger, 1991; Stafstrom et al., 1985), indicating that MT stimulation might induce calcium-dependent spikes. In addition, optogenetic inhibition of MT input to layer 1 seems to further increase the proportion of induced calcium-dependent spikes.

Although a previous study reported long-term effects upon sustained optogenetic inhibition of axon terminals such as an increase in spontaneous neurotransmitter release (Mahn et al., 2016), we did not observe any rebound spiking after optogenetic inhibition of MT axon terminals for as long as 20 secs. We never inhibited axon terminals for longer than 20 secs,

386 indicating that the results outlined above were not caused by unexpected side effects from
387 optogenetic inhibition (Figure 3F). Overall, our results are in line with previous studies that
388 used the same virus (AAV5-CAG-ArchT-GFP) or the same viral construct as serotype 2
389 (AAV2-CAG-ArchT-GFP) to inhibit axon terminals, which showed robust behavioral effects
390 (Stefanik et al., 2016; Stefanik and Kalivas, 2013) and partly confirmed that the virus is
391 suitable for inhibiting axon terminals (Ozawa et al., 2017; Stefanik et al., 2013a, 2013b).
392

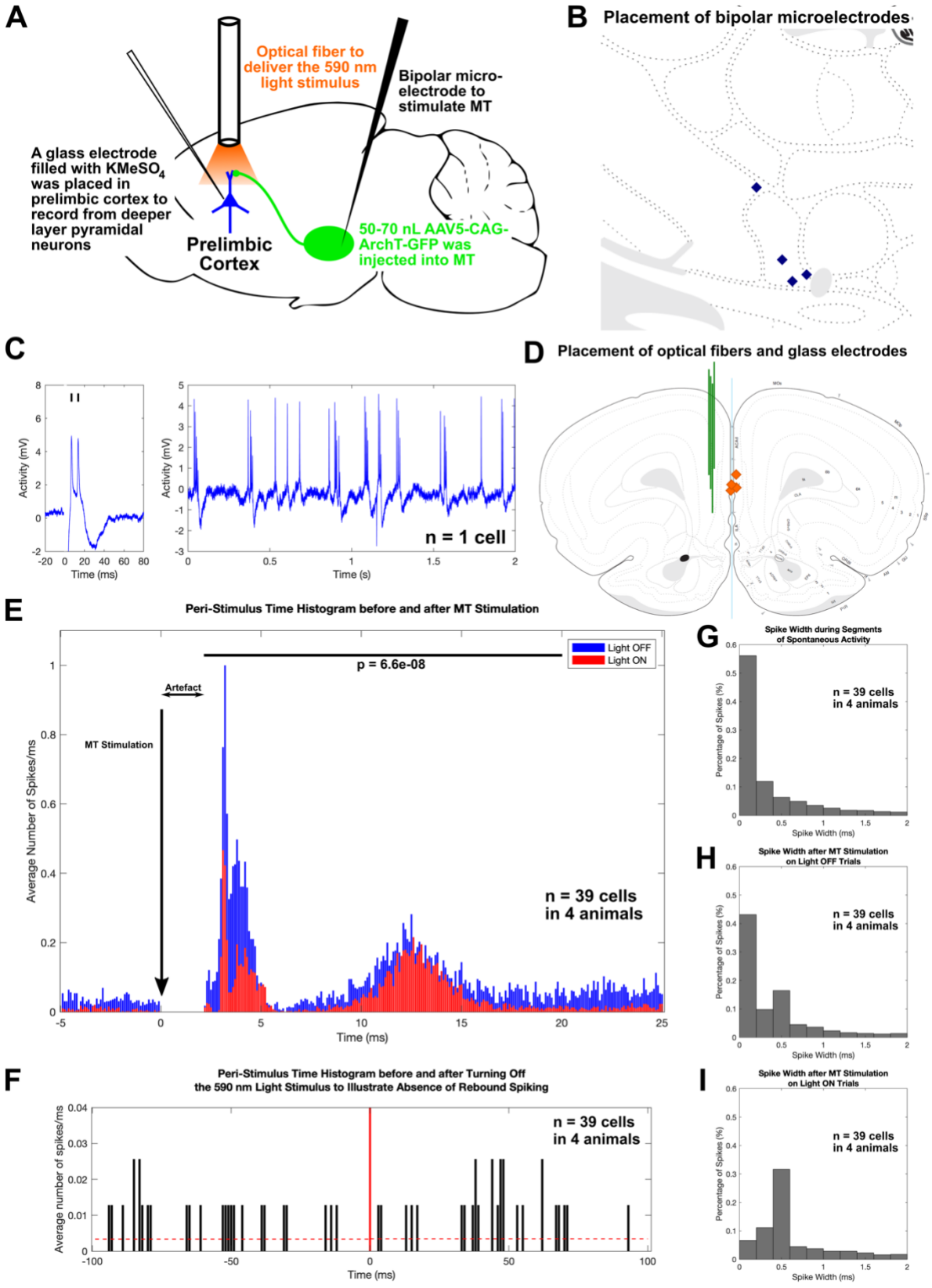

Figure 3. In anesthetized rats, MT stimulation induced a response in deep layer prelimbic neurons and optogenetic inhibition of MT input to prelimbic cortex reduced the response. A-

MT was injected with 50-70 nL AAV5-CAG-ArchT-GFP. A glass electrode was used to record from neurons in deep layers of prelimbic cortex. MT was stimulated with a bipolar microelectrode. A 590 nm LED was placed in prelimbic cortical layer 1 to optogenetically inhibit MT axon terminals. B- Positioning of bipolar stimulating electrodes in MT. C- Neuronal response evoked by MT stimulation (left) and spontaneous activity recorded from one neuronal cluster (right). Extracellular spikes are marked by a small black line above the spike. D- Positioning of optical fiber tips (orange) and glass electrode tracks (green) in prelimbic cortex. E- Peri-stimulus time histograms show extracellular responses from 5 ms prior until 25 ms after MT stimulation in light OFF (blue) or ON trials (red). F- A peri-stimulus time histogram illustrates spontaneous neuronal activity in deep layers of prelimbic cortex. The vertical red line marks the time the 590 nm light was turned off. The red dotted lines indicate the mean number of spikes in the 100 ms before and after the light was turned off. G- Histogram of the width of spikes during segments of spontaneous activity, after MT stimulation on H- light OFF trials, or I- light ON trials.

MT input to prelimbic layer 1 inhibitory interneurons contributes to the regulation of neuronal activity in deep layers of prelimbic cortex

The ventromedial thalamus, one of the nuclei that make up MT, provides input to both prelimbic pyramidal neurons and prelimbic layer 1 inhibitory interneurons (Sieveritz and Arbuthnott, 2020). Hence, we were interested in whether prelimbic layer 1 inhibitory interneurons contribute to MT-mediated regulation of neuronal activity in deep layers of prelimbic cortex. We previously proposed that MT input regulates the activity of prelimbic layer 1 inhibitory interneurons. We further proposed that, in turn, layer 1 inhibitory interneurons regulate a network of cortical inhibitory interneurons, which ultimately regulates the activity of deep layer pyramidal neurons (Sieveritz and Arbuthnott, 2020).

To test our prediction, we stimulated MT and simultaneously inhibited layer 1 inhibitory interneurons using optogenetics. In three 9- to 10-week-old Sprague-Dawley rats, we placed small unilateral injections of 10-20 nl AAV5-CAG-ArchT-GFP in prelimbic cortical layer 1. Given that prelimbic cortical layer 1 only contains inhibitory interneurons (Kubota, 2014) and no pyramidal neurons, this resulted in specific expression of AAV5-CAG-ArchT-GFP in prelimbic layer 1 inhibitory interneurons (Figure 4C). We observed no expression of the virus in pyramidal neurons or any other neurons in deeper layers of prelimbic cortex. Similar to the previous experiment, an optical fiber that was coupled to a 590 nm LED was inserted through the contralateral hemisphere and placed in ipsilateral prelimbic cortical layer 1. To stimulate MT, a bipolar stimulating electrode was placed in ipsilateral MT. A glass electrode filled with 3.0M potassium methyl sulfate ($KMeSO_4$) and goat anti-rat Alexa Fluor 594 (dilution between 1:50 to 1:200) was lowered into deep layers of ipsilateral prelimbic cortex to record extracellular neuronal activity (Figure 4A). Figure 4B and 4D illustrate the placement of optical fibers, bipolar stimulating electrodes and glass recording electrodes.

As outlined for the previous experiment, we stimulated ipsilateral MT for 0.5 ms at -5 mA to induce responses in neuronal clusters in deep layers of prelimbic cortex (light OFF trials). Figure 4E shows an example of evoked spikes and of recorded spontaneous activity. When MT stimulation evoked a response, we simultaneously delivered 590 nm light to prelimbic cortical layer 1 to induce optogenetic inhibition in layer 1 inhibitory interneurons (light ON trials). Optogenetic inhibition of layer 1 inhibitory interneurons resulted in a decrease of evoked responses (Figure 4F). The average number of extracellular spikes per millisecond observed between 2 and 20 ms after MT stimulation decreased significantly; independent of the strength of MT stimulation (paired t-test; for MT stimulation of -5 mA: p=1.2e-6, df=36; for -3 mA: p=1.2e-5, df=36; for -1 mA: p=0.8e-2, df=36). Overall, our result indicates that

prelimbic layer 1 inhibitory interneurons contribute to MT-mediated regulation of deep layer neurons in prelimbic cortex.

Evoked spikes had comparable widths in segments of spontaneous activity and after MT stimulation (Figure 4G and 4H), but were wider when MT stimulation was paired with optogenetic inhibition of layer 1 inhibitory interneurons (Figure 4I). Given that calcium-dependent spikes in cortex are wider (De La Peña and Geijo-Barrientos, 2000; Pockberger, 1991; Stafstrom et al., 1985), inhibition of layer 1 inhibitory interneurons seems to increase the number of MT-induced calcium-dependent spikes. The result further underlines the importance of layer 1 inhibitory interneurons in processing of MT input to prelimbic cortex.

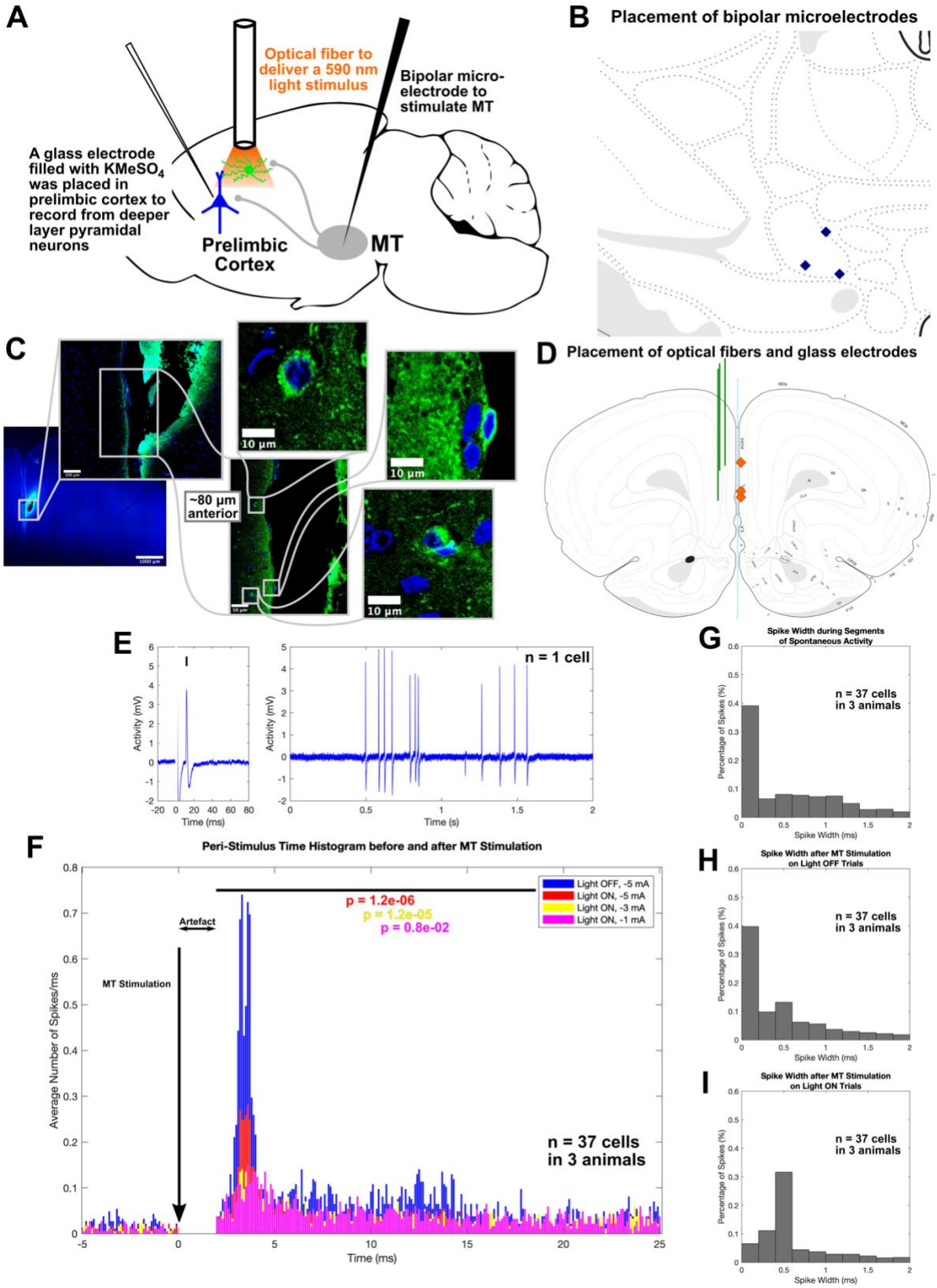

Figure 4. In anesthetized rats, optogenetic inhibition of layer 1 inhibitory interneurons in prelimbic cortex reduced extracellular responses to MT stimulation. A- Prelimbic cortical layer 1 was injected with 10-20 nL of AAV5-CAG-ArchT-GFP. A glass electrode was used

to record from neurons in deep layers of prelimbic cortex. MT was stimulated with a bipolar microelectrode. A 590 nm LED was placed in prelimbic cortical layer 1 to optogenetically inhibit layer 1 inhibitory interneurons. B- Positioning of bipolar stimulating electrodes in MT. C- The optical fiber tip was located in and virus expression was limited to inhibitory interneurons (green) in prelimbic cortical layer 1. D- Positioning of optical fiber tips (orange) and glass electrode tracks (green). E- Neuronal response evoked by MT stimulation (left) and spontaneous activity recorded from the same neuronal cluster (right). Extracellular spikes are marked by a small black line above the spike. F- Peri-stimulus time histograms show extracellular responses extracellular responses in light OFF trials from 5 ms prior until 25 ms after MT stimulation at -5 mA (blue), and in light OFF trials after MT stimulation at -5 mA (red), -3 mA (yellow) and -1 mA (pink). G- Histogram of the width of spikes during segments of spontaneous activity, after MT stimulation on H- light OFF trials, or I- light ON trials.

Discussion

Optogenetic inhibition of MT axon terminals in prelimbic cortical layer 1 biased rats towards a high cost-high benefit option, indicating that MT input to prelimbic cortex is necessary for cost-benefit decision-making. Rats were still able to accurately discriminate high and low benefit, and high and low cost options, indicating that MT input to prelimbic cortex is not necessary to process benefit or cost. However, it is crucial for trade-off choices that require rats to integrate multiple, conflicting reward values. Such integration of reward values might happen in MT before the outcome of such a computation is transmitted to prelimbic cortex. Alternatively, MT input to prelimbic cortical layer 1 might modulate inputs from other brain regions to prelimbic cortex that drive integration of multiple, conflicting reward values. The latter explanation is supported by findings that MT input to prelimbic cortex is primarily

modulatory (Collins et al., 2018). The former explanation highlights a long debate on whether thalamic nuclei only relay information between specific brain areas, or whether they perform computations on incoming streams of information and transmit the outcome of these computations to other brain areas. Research in the sensory domain demonstrated that sensory thalamic nuclei can integrate two incoming streams of signals (Saalmann and Kastner, 2011; Wolff et al., 2021). More recent research on the central thalamus, a region that borders with MT, has further shown that thalamic nuclei concerned with motor control might likewise integrate two streams of incoming signals (Matsuyama and Tanaka, 2021). In our case, MT might integrate benefit and cost before transmitting the outcome to prelimbic cortex. When no integration of the two is required, inhibition of MT input to prelimbic cortex does not affect choice behavior. However, when integration is required, inhibition of MT input to prelimbic cortex biases rats towards a high cost-high benefit option. Independent of which of the two explanations is correct, our results demonstrate that MT input to prelimbic cortex is necessary to integrate multiple, conflicting reward values. We thus extend previous findings in mice that showed MT activity is correlated with action initiation (Gaidica et al., 2018) and reciprocal projections between MT and anterior lateral motor cortex play a role in sensory discrimination (Guo et al., 2017).

We uncovered a possible mechanism by which MT input to prelimbic cortex might regulate cost-benefit decision-making. Corticostriatal pyramidal neurons in deep layers of prelimbic cortex are known to be involved in cost-benefit decision-making (Friedman et al., 2015). We demonstrated that optogenetic inhibition of MT input to prelimbic cortex as well as inhibition of prelimbic layer 1 inhibitory interneurons reduced extracellular responses of neurons in deep layers of prelimbic cortex. We previously reported that about 80% of MT axon terminals that project onto prelimbic pyramidal neurons, project onto corticostriatal

pyramidal neurons (Sieveritz and Arbuthnott, 2020). Given that MT stimulation evoked a response in the neuronal clusters that we recorded from, it is likely that we recorded from clusters of corticostriatal pyramidal neurons. Taking this into consideration, we propose a two-fold mechanism to explain how MT input to prelimbic cortex regulates cost-benefit decision-making: 1) MT input directly regulates the activity of corticostriatal pyramidal neurons; and 2) MT input regulates the activity of layer 1 inhibitory interneurons, which induces feedforward inhibition in a network of cortical inhibitory interneurons. In turn, corticostriatal pyramidal neurons are disinhibited. When layer 1 inhibitory interneurons are inhibited, as was the case in our experiment, corticostriatal pyramidal neurons are no longer disinhibited and their activity is reduced. We further propose that the resulting decrease in corticostriatal pyramidal activity caused the observed bias towards a high cost-high benefit option (Figure 5). We believe that such a mechanism is likely, given that direct optogenetic inhibition of corticostriatal pyramidal neurons similarly induced a bias towards a high cost-high benefit option (Friedman et al., 2015).

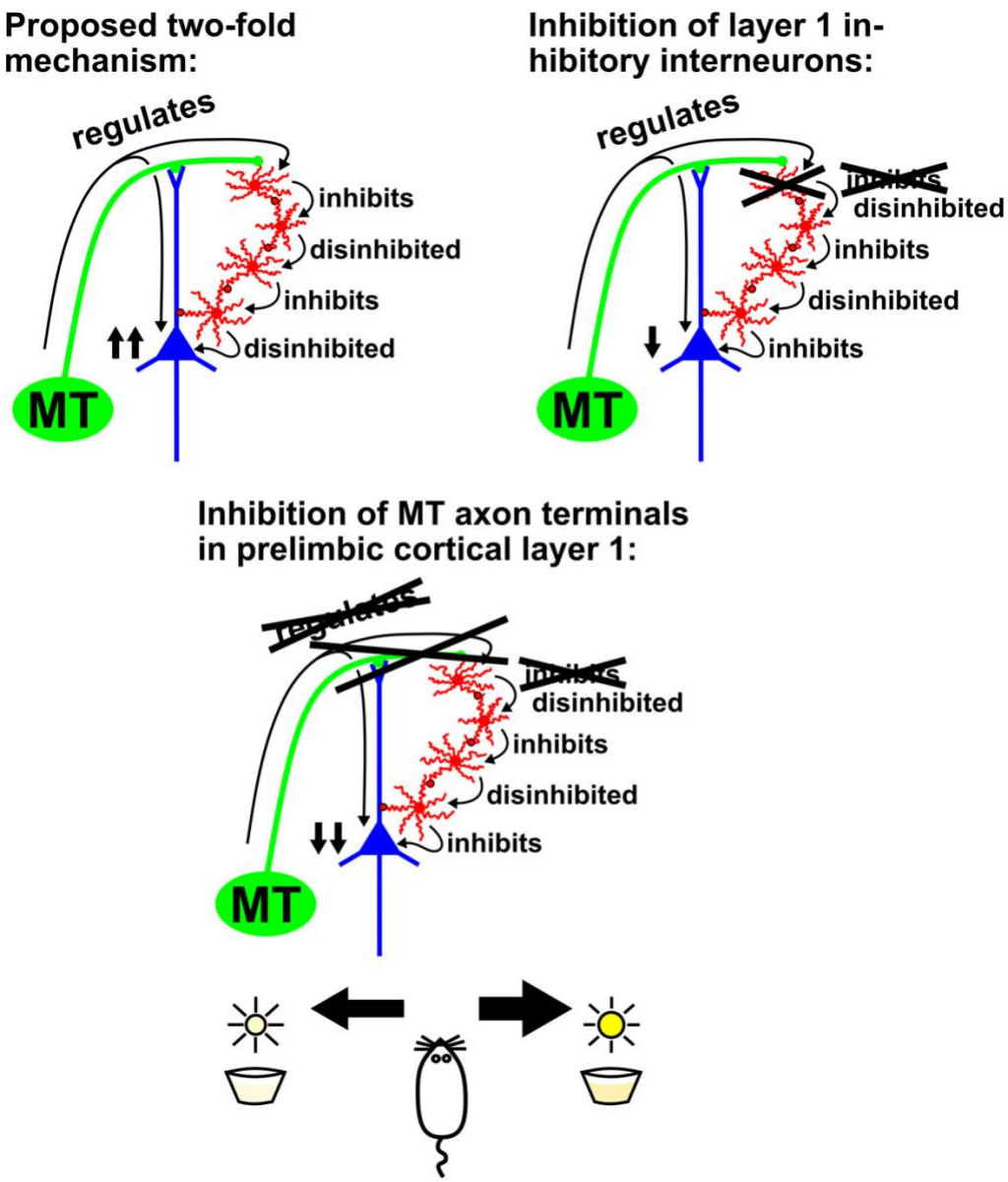

526

527 **Figure 5.** Proposed two-fold mechanism. MT input to prelimbic cortex regulates the activity
528 of corticostriatal pyramidal neurons directly as well as indirectly via a network of cortical
529 inhibitory interneurons. When layer 1 inhibitory interneurons are optogenetically inhibited,
530 corticostriatal pyramidal neurons are no longer disinhibited and their activity is reduced.
531 When MT axon terminals in prelimbic cortical layer 1 is optogenetically inhibited, the
532 activity of corticostriatal pyramidal neurons is reduced due to missing MT input as well as
533 due to them being inhibited by the network of cortical inhibitory interneurons. This causes
534 the observed behavioral bias towards a high cost-high benefit option.

MT input might regulate the activity of corticostriatal pyramidal neurons through subthreshold excitation. We used high negative currents (-5 mA) that exceed those observed under physiological conditions, to evoke responses in neuronal clusters in deep layers of prelimbic cortex. In contrast, a previous study showed that optogenetic stimulation of MT axon terminals in prelimbic cortex *in-vitro* does not evoke action potentials in deep layer pyramidal neurons and only subthreshold excitation was observed (Collins et al., 2018). Therefore, MT might gate inputs from other subcortical sources to corticostriatal pyramidal neurons in prelimbic cortex by regulating subthreshold excitation of these neurons. A similar mechanism was observed for the mediodorsal thalamic nucleus, which gates responses in prefrontal cortical neurons that were evoked by stimulation of the hippocampal output tract (Floresco and Grace, 2003). Alternatively, MT might regulate the activity of corticostriatal pyramidal neurons by long-term potentiation or depression, a mechanism that has been demonstrated for posterior medial thalamic input to barrel cortex (Williams and Holtmaat, 2019).

In contrast to optogenetic inhibition of MT axon terminals in prelimbic cortical layer 1, global chemogenetic inhibition of MT striatal-projecting neurons did not alter the choice behavior of our rats. These results were surprising to us, first, because MT striatal-projecting neurons target striatal fast-spiking interneurons, which are associated with cost-benefit decision-making (Friedman et al., 2015). Second, because MT axons projecting to striatum branch off from MT axons that continue to cortex (Elena Erro et al., 2002; Kuramoto et al., 2009). One would expect that at least some of the transfected MT striatal-projecting neurons have axons that continue to prelimbic cortex. One would further expect that chemogenetic inhibition of these transfected MT neurons would reproduce the results observed with optogenetic inhibition. There are several possible reasons why this is not the case. First, we

might not have transfected enough MT striatal-projecting neurons to induce a behavioral bias. However, considering the used parameters, when using optogenetic inhibition we were inhibiting a relatively small number of MT axon terminals in prelimbic cortical layer 1. Therefore, chemogenetic inhibition of even a small number of transfected MT striatal-projecting neurons should have induced a behavioral bias. Second, the observed behavioral bias might have exclusively relied on optogenetic inhibition of axon terminals from those MT neurons that do not send branches to striatum. Third, global chemogenetic inhibition of MT striatal-projecting neurons that continue to cortex might reduce activity in both striatum and cortex. The observed change in choice behavior might thus rely on an imbalance of activity between cortical versus striatal activity. Global chemogenetic inhibition might reduce activity in both cortex and striatum, but might not cause an imbalance in activity between the two brain regions. However, more research will be needed to determine whether this is the case. Based on our current results, we conclude that MT input to striatum is not involved in cost-benefit decision-making.

Aberrant decision-making is a symptom in anxiety (Aupperle and Paulus, 2010), depression (Amemori and Graybiel, 2012) and chronic stress (Schwabe and Wolf, 2009; Sousa and Almeida, 2012). Chronic stress biased rats towards high cost-high benefit options (Friedman et al., 2017), similar to what we observed when we inhibited MT axon terminals in prelimbic cortical layer 1. Given that optogenetic inhibition of MT input to prelimbic cortex emulates a behavioral phenotype observed under chronic stress, MT might play a crucial role in regulating stress. Patients with major depressive disorder exhibited aberrant task-related prefrontal cortical activity on an approach avoidance task that required integration of benefit and cost (Ironside et al., 2020). Hence, MT input to prefrontal cortex might also contribute to depression.

585 Overall, our results suggest that, in addition to MT being involved in diseases related to
586 motor control such as Parkinson's disease (Brazhnik et al., 2016), MT might also be crucial in
587 disorders associated with aberrant decision-making. Our results provide evidence that the role
588 of MT in cognition must be reevaluated. Further studies will be necessary to understand the
589 contribution of thalamic nuclei to cognition.
590
591 **Materials and Methods**
592 *1. Animals*
593 53 male Sprague-Dawley rats (Charles River Laboratories, Japan) between 4 and 11 weeks of
594 age were used. Table 1 provides a detailed overview of the numbers and ages of rats used in
595 each experiment. Rats were single housed in a climate-controlled vivarium, maintained on a
596 12h light/dark cycle. Rats used in behavioral experiments were housed on a reversed light
597 cycle (lights on at 2200h, lights off at 1000h). Rats used in electrophysiological experiments
598 were either housed on a regular light cycle (lights on at 0700h, lights off at 1900h) or on a
599 reversed light cycle (lights on at 2200h, lights off at 1000h). Food and water were available
600 *ad libitum*. Behavioral experiments were conducted within the last 4 hours of the light cycle
601 or during the dark cycle. Rats were excluded from the study, when virus injections extended
602 beyond the target brain region or when the tip of optical fibers was located outside of the
603 target brain area. In addition, rats used in behavioral experiments were excluded from the
604 study, if they failed to reach the behavioral criteria on any of the three decision-making tasks
605 as specified below. The required number of animals for behavioral experiments was predicted
606 a priori based on a similar study conducted in the past (Friedman et al., 2015), but did not
607 estimate it a priori based on assumptions. The required number of cells for
608 electrophysiological experiments in anesthetized rats was also predicted based on previous
609 studies (Brecht and Sakmann, 2002; Martin-Cortecero and Nuñez, 2016; Yuan et al., 1985).

610

Experiment	**Age**	**Number of Rats**
Optogenetic inhibition of MT axon terminals in prelimbic cortex on decision-making tasks	Habituation and behavioral training started at 4-5 weeks, surgery performed at 9 weeks and behavioral testing performed at 11 and 12 weeks	22
Chemogenetic inhibition of MT striatal-projecting neurons on decision-making tasks	Habituation and behavioral training started at 4-5 weeks, surgery performed at 9 weeks and behavioral testing performed at 12 weeks	24
Electrophysiology in anesthetized rats to explore effects of MT stimulation and simultaneous MT axon terminal inhibition on deeper layer pyramidal neurons in prelimbic cortex	Surgery at 9 weeks and electrophysiology performed at 11 weeks	1
	Surgery at 10 weeks and electrophysiology performed at 12 weeks	2
	Surgery at 11 weeks and electrophysiology performed at 13 weeks	1

Electrophysiology in anesthetized rats to explore effects of MT stimulation and simultaneous inhibition of layer 1 inhibitory interneurons on deeper layer pyramidal neurons in prelimbic cortex	Surgery at 9 weeks and electrophysiology performed at 11 weeks	1
	Surgery at 10 weeks and electrophysiology performed at 12 weeks	2

Table 1. Overview of Used Rats. Age and number of rats used in each experiment.

All applicable international, national, and/or institutional guidelines for the care and use of animals were followed. All procedures performed in studies involving animals were in accordance with the ethical standards of the Okinawa Institute of Science and Technology Graduate University and were approved by the Animal Care and Use Committee of the Okinawa Institute of Science and Technology Graduate University (protocols #2016-131 and #2018-212).

2. Behavioral Tasks

Forty-six 4- to 5-week-old Sprague-Dawley rats were trained on a benefit-benefit, cost-cost and cost-benefit decision-making task. Behavioral tasks were modeled after similar behavioral tasks presented in a previous study (Friedman et al., 2015). Rats were trained 6 to 7 days a week for up to 24 days.

2.1 Apparatus

Behavioral training and testing were conducted in three standard modular test chambers for rats, two of which had a drug infusion top (Med Associates, ENV-008 and ENV-008CT).

Each test chamber was enclosed in a custom-made sound-attenuating cubicle and connected to a personal computer by a SmartCtrl connection panel (Med Associates, SG-716B) and a SmartCtrl interface module (Med Associates, DIG-716B). In each test chamber a modified pellet/liquid drop receptacle (Med Associates, ENV-200R3M) was located at the center of the front panel. Two small food trays were attached to the front of the modified receptacle and two blunt needles were placed on top of these small food trays to deliver two different liquids into them. Liquids were delivered using two single speed syringe pumps (Med Associates, PHM-100-3.33) and 50 ml lock type plastic syringes (Terumo). Two retractable levers (Med Associates, ENV-112CM) were placed on each side of the modified receptacle. A white stimulus light (Med Associates, ENV-221M) was mounted above each lever. Stimulus lights were connected to a two level stimulus light fader controller (Med Associates, ENV-226) and could reach a maximum intensity of 200 lx or be reduced to an intensity of 1 lx. Each test chamber was further fitted with a 2900 Hz sonalert module (Med Associate, ENV-223AM), which was mounted in the upper left corner of the front response panel. A 15W LED light (12VMonster, P-15W-E27-CW-12V85V) was placed above each test chamber in a 12V lamp holder (12VMonster, WIRE-E27-2.1MM-2.5M-BLACK) and connected to a SmartCtrl connection panel (Med Associates, SG-716B) by a custom-made electrical circuit board. The SmartCtrl connection panel was connected to a personal computer by a SmartCtrl interface module (Med Associates, DIG-716B). Chronically implanted LED fiber optics, which emitted 590 nm light (TeleLC-Y-8-250, Bio Research Center Co., Ltd.), were controlled by a wireless receiver (TeleR-1-C, Bio Research Center Co., Ltd.). Prior to each behavioral training session, a wireless receiver was secured to the head of each animal and connected to the implanted LED fiber optic. Each wireless receiver was remote-controlled by an infrared signal using a Teleopto Remote (Bio Research Center Co., Ltd.) and a Teleopto Emitter (Bio Research Center Co., Ltd.). Both were placed behind each test chamber. Teleopto Remotes

were connected to a personal computer by a passive TTL connection panel (Med Associates, SG-726-TTL) and a SuperPort TTL output interface module (Med Associates, DIG-726TTL-G). The hardware was operated using the Med-PC IV software suite (Med Associates, SOF-735).

2.2 Habituation and Lever Pressing Training

Rats were put on a reversed light cycle (lights on at 2200h, lights off at 1000h) at least 7 days prior to the start of behavioral training, and were handled by the experimenter for at least 3 days out of the 5 days prior to the start of behavioral training. Rats were habituated to 20% sweetened condensed milk diluted in tap water prior to the start of behavioral training. For each animal, 20 mL of 20% sweetened condensed milk diluted in tap water were placed in the home cage on 2 consecutive days out of the 5 days prior to the start of behavioral training.

We first trained rats to press one of two retractable levers using a modified continuous reinforcement schedule. Each training session started with a 5-second-long tone stimulus (2900 Hz, 65db) and 5 secs later one of the two retractable levers was presented to the animal. Each lever press resulted in retraction of the lever, delivery of 0.1 mL of 20% sweetened condensed milk diluted in tap water and presentation of the stimulus light above the lever at reduced intensity (1 lx) for 10 secs. Once the stimulus light was turned off, a 10-second-long pause occurred. Next, we presented another 5-second-long tone stimulus (2900 Hz, 65db) to the animal and after another 5 secs the same retractable lever was presented to the animal again. Rats were presented with one 40-minute-long training session each day for up to 12 days. In each training session only one lever was presented to the animal. The presented lever was alternated each day, unless rats had previously reached criterion on one

of the two levers, i.e. performed 30 lever presses on the lever in 40 mins. If this was the case, on subsequent days rats were solely trained on the lever that they had not yet reached criterion on. For each of the two levers rats had a total of 6 days to reach criterion, i.e. a maximum of 12 days in total. If rats did not press the presented lever at least one time on two consecutive days, the behavior of rats was shaped by the experimenter. The animal's paw was placed on the lever and moved downwards to press the lever. Afterwards the animal was moved to the food tray to collect the reward. Shaping was performed for 5 consecutive lever presses. Rats reached criterion on the lever pressing training in an average of 5.1 +/- 2.3 days (mean +/- standard deviation).

2.3 Behavioral Training

Once rats reached criterion on both levers in the lever pressing training, they were trained to perform the benefit-benefit, cost-cost and cost-benefit decision-making task. Rats were always trained first on the benefit-benefit, then on the cost-cost, and last on the cost-benefit decision-making task. Each day rats completed 40 trials in the decision-making task that they were currently trained on. Each trial started with a 5-second-long tone stimulus (2900 Hz, 65 dB) or, in the cost-cost and cost-benefit decision-making task a 5-second-long tone stimulus paired with a 100-millisecond-long bright light flash (1.75 kLx). After an additional 5 secs both retractable levers were presented to the animal for up to 10 secs or until a response was made. If the animal made no response within 10 secs, both levers were retracted, and the trial was counted as omitted.

In each of the three tasks rats were presented a choice between two levers and each lever was associated with a specific combination of benefit and cost. In the benefit-benefit decision-making task, pressing either of the two levers resulted in the presentation of a low cost, i.e. a

dim light at 1 lx, for 10s. However, pressing one lever resulted in the delivery of a high benefit (0.1 mL of sweetened condensed milk diluted at 20%), while pressing the other lever resulted in delivery of a low benefit (for training 0.1 mL of sweetened condensed milk diluted at 5%, for testing 0.1 mL of sweetened condensed milk diluted at 1-19% or pure tap water). In the cost-cost decision-making task pressing either of the two levers resulted in delivery of a high benefit (0.1 mL of sweetened condensed milk diluted at 20%). However, pressing one lever was associated with presentation of a high cost, i.e. a bright light stimulus (1.75 kLx), for 10s. In contrast, pressing the second lever was associated with presentation of a low cost, i.e. a dim light (1 lx), for 10s. In the cost-benefit decision-making task one lever was associated with a high cost-high benefit option and pressing the lever resulted in a 10-second-long presentation of a bright light stimulus (1.75 kLx) paired with delivery of a high benefit (0.1 mL of sweetened condensed milk diluted at 20%). In contrast, the other lever was associated with a low cost-low benefit option and pressing that lever resulted in a 10-second-long presentation of a dim light (1 lx) paired with delivery of a low benefit (for training 0.1 mL of sweetened condensed milk diluted at 5%, for testing 0.1 mL of sweetened condensed milk diluted at 1-19% or pure tap water). Each trial was followed by an inter-trial interval of 25 secs.

Rats were trained on each of the three decision-making tasks for at least 3 days and until criterion was reached. Rats that did not reach criterion after 6 days of training on the benefit-benefit and cost-benefit decision-making task, or after 8 days of training on the cost-cost decision-making task were excluded from the experiment. Criterion on all three decision-making tasks was that less than 20% of trials were omitted. In addition, in the benefit-benefit decision-making task rats had to choose the high benefit option and in the cost-cost decision-making task the low cost option on at least 52% of the trials. Overall, 53.7% of rats were able

to learn the task. Reported animal numbers only include rats that reached criterion and were included in the data analysis. Across rats that learned all three decision-making tasks, criterion was reached in an average of 3.3 +/- 0.7 days on the benefit-benefit decision-making, in an average of 4.3 +/- 1.7 days on the cost-cost decision-making task, and in an average of 2.4 +/- 1.2 days on the cost-benefit decision-making task (mean +/- standard deviation).

The perceived value of different dilutions of sweetened condensed milk offered as a benefit differed across rats. Hence, we used the first three days of behavioral training on the cost-benefit decision-making task to estimate an individual dilution of sweetened condensed milk for each animal such that rats would choose both, the high cost-high benefit and the low cost-low benefit option in approximately 50% of cost-benefit decision-making trials. The dilution of the sweetened condensed milk offered as a low benefit was systematically varied across the 120 trials presented over the first 3 days of behavioral training on the cost-benefit decision-making task. The dilution was reduced every 20 trials starting at 13% followed by 11%, 8%, 5%, 2% and then pure tap water. For each dilution the percentage of trials that the animal chose the low cost-low benefit option out of the overall number trials that were not omitted was calculated and a psychometric curve was fitted to the data to estimate the best dilution of sweetened condensed milk for each animal. The psychometric curve was fitted using the FitWeibull function from the PsychoPy package (Peirce, 2007) under Python 2.7 (since PsychoPy is no longer functional under Python 2.7, the source code that is made available was updated to run under Python 3). For each animal, guesses for the threshold and slope of the psychometric curve were made by the experimenter based on the collected data. Usually, the guess for the threshold was equal to the dilution at which rats chose the low cost-low benefit option in about 50% of the trials. The initial guess for the slope was 2, but if no

optimal parameters for the psychometric curve were found by the function, the parameter for the slope was increased to 5 and then doubled until optimal parameters were determined. The resulting dilution of sweetened condensed milk was rounded to the nearest whole number. Given that the individual dilution of sweetened condensed milk for each animal was determined during training on the cost-benefit decision-making task, the individual dilution could not be used for initial training on the benefit-benefit decision-making task. Thus, on the benefit-benefit decision-making task all rats were trained with a low benefit of 0.1 ml sweetened condensed milk diluted at 5%.

2.4 Behavioral Testing

2.4.1 Optogenetic Inhibition of MT axon terminals in prelimbic cortical layer 1

Once rats had reached criterion on all three decision-making tasks and were 9 weeks of age, 50-70 nl of either AAV5-CAG-ArchT-GFP (titer ≥ 7×10^{12} vg/mL; gift from Edward Boyden and purchased through UNC Vector Core; now commercially available from Addgene viral preparation #29777-AAV5; http://n2t.net/addgene:29777; RRID:Addgene_29777) or the control virus AAV5-CAG-GFP (titer ≥ 7×10^{12} vg/mL; gift from Edward Boyden and purchased through UNC Vector Core; now commercially available from Addgene viral preparation #37825-AAV5; http://n2t.net/addgene:37825; RRID:Addgene_37825) were injected into MT. In the same aseptic surgery, a short optical fiber attached to a 590 nm light emitting diode (LED fiber optic) was implanted through the contralateral hemisphere into ipsilateral prelimbic cortical layer 1. As described above, LED fiber optics were controlled by wireless receivers. The maximum light intensity that was reached using the wireless receivers and LED fiber optics was between 0.7-1.2 mW. Given that LED fiber optics had a diameter 250 μm, the emitted 590 nm light reached approximately 3-6 mW/mm^2.

After a 12- to 16-day-long recovery period that followed surgery, rats' choice behavior on each decision-making task was assessed over a period of 9 days. For each decision-making task, rats were presented with 40 trials per day on 3 consecutive days. The first 20 trials were presented without delivery of the 590 nm light (light OFF) and the last 20 trials were paired with delivery of the 590 nm light (light ON), which induced optogenetic inhibition of MT axon terminals in prelimbic cortical layer 1 in ArchT rats. In total, we presented rats with 60 light OFF and 60 light ON trials on each decision-making task. The 590 nm light was turned on at the same time as the tone stimulus and remained on until rats made a choice or until the levers were retracted, i.e. a maximum of 20 secs. We decided on a block design for presentation of light OFF and ON trials, since a previous study suggested that sustained optogenetic inhibition of axon terminals may cause unexpected long-term effects such as an increase in spontaneous neurotransmitter release (Mahn et al., 2016). Hence, light ON trials were always presented after light OFF trials. All rats were first tested on the benefit-benefit, then on the cost-cost and last on the cost-benefit decision-making task. We presented the decision-making tasks in this specific order, to increase rats' retention of the tasks. A timeline for behavioral testing is provided in Figure 6.

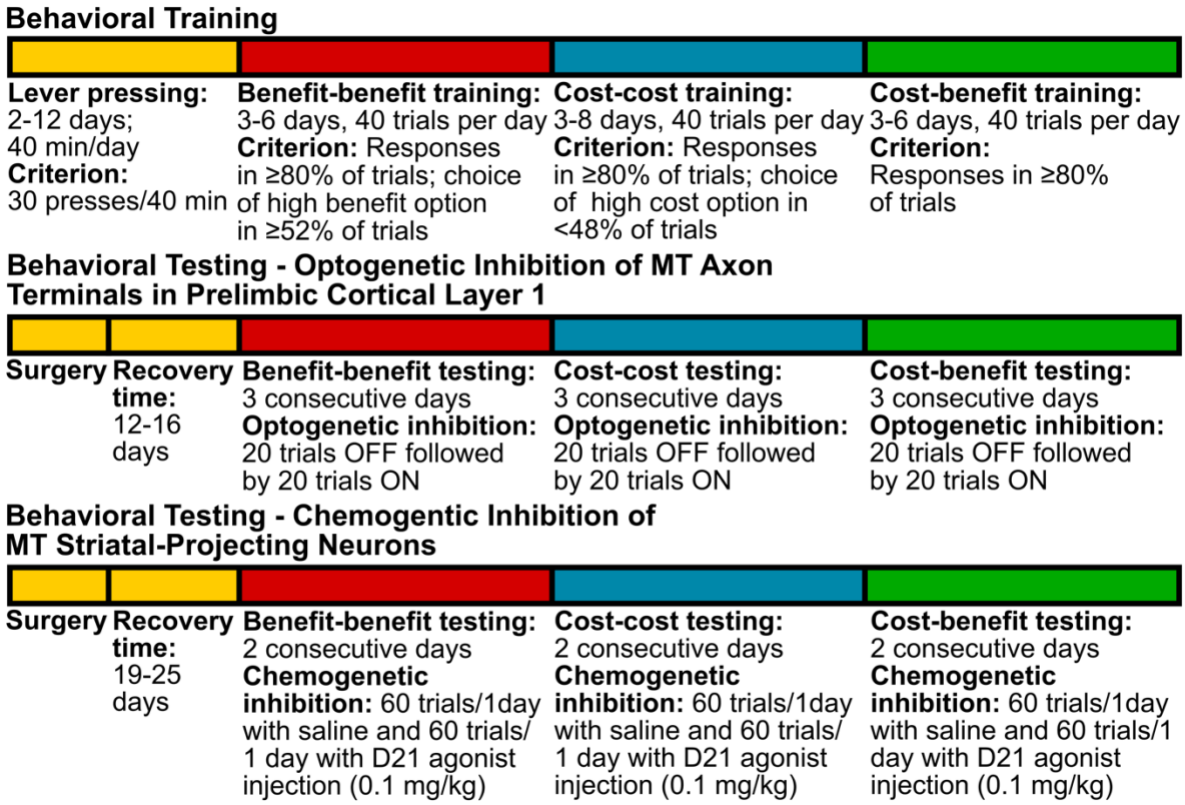

Figure 6. Timeline of behavioral training and testing for behavioral experiments assessing the effect of optogenetic inhibition of MT axon terminals in prelimbic cortical layer 1 and chemogenetic inhibition of MT striatal-projecting neurons.

2.4.2 Chemogenetic Inhibition of MT Thalamostriatal Projection Neurons

Once rats had reached criterion on all three decision-making tasks and were 9 weeks of age, 50-60 nl of either AAV5-hSyn-DIO-hM4D(Gi)-mCherry (titer ≥ 7×10^{12} vg/mL; gift from Bryan Roth, Addgene viral preparation #44362-AAV5; http://n2t.net/addgene:44362; RRID: Addgene_44362) or the control virus AAV5-hSyn-DIO-mCherry (titer ≥ 7×10^{12} vg/mL; gift from Bryan Roth, Addgene viral preparation #50459-AAV5; http://n2t.net/addgene:50459; RRID: Addgene_50459) were injected into MT, followed by an injection of 300 nl of AAVrg-pmSyn1-EBFP-Cre (titer: 6×10^{12} vg/mL; gift from Hongkui Zeng; Addgene viral preparation #51507-AAVrg; RRID: Addgene_51507) into striatum. After a 19- to 25-day-long recovery period that followed surgery, rats' choice behavior on each decision-making

task was assessed over a period of 6 days. All rats were first tested on the benefit-benefit, then on the cost-cost and last on the cost-benefit decision-making task. For each decision-making task rats were presented with 60 trials per day on two consecutive days. One of the two days rats received intraperitoneal injections of D21 agonist diluted in saline (1 mg/kg), while on the other day rats were injected with the same amount of saline. Injections were given 10-15 minutes prior to the experiment. A timeline for behavioral testing is provided in Supplementary Figure 5.

2.5 Randomization of Animal Groups

For lever pressing training for one group of rats the left lever was presented on the first day and the right lever on the second day, while for a second group of rats the right lever was presented on the first day and the second lever was presented on the second day. For behavioral training and testing for one group of rats the left and for a second group of rats the right lever was associated with the high benefit, high cost and high cost-high benefit option. The lever on the opposite side was associated with the other choice option. Rats were pseudo-randomly assigned to these groups. Rats were further pseudo-randomly assigned to being injected with AAV5-CAG-ArchT-GFP/AAV5-hSyn-DIO-hM4D(Gi)-mCherry or the corresponding control virus.

2. Surgeries

Virus injections, LED fiber optics or both were placed in 9- to 11-week-old male Sprague-Dawley rats. Rats were anesthetized with 5% isoflurane delivered with room air (0.5-1 L/min; Small Animal Anesthetizer, Muromachi, MK-A100, Japan). Rats were positioned in a stereotaxic frame (Narishige, SR-5R-HT, Japan) and anesthesia was maintained at 2% isoflurane delivered with room air (0.5-1 L/min). Virus injections were performed with a

836 Hamilton syringe (Neuros Syringe, 0.5 µL, Neuros Model 7000.5 KH, point style 3,
837 Hamilton, 65457-01, United Kingdom or Neuros Syringe, 1.0 µL, Neuros Model 7001 KH,
838 point style 3, Hamilton, 65458-01, United Kingdom) at an injection speed of 100 nL/min and
839 the syringe remained at the target location for 10 min after the injection before it was slowly
840 retracted from the brain. All experiments involving recombinant DNA were approved by the
841 Biosafety Committee of the Okinawa Institute of Science and Technology Graduate
842 University (protocol #RDE-2017-003) and all applicable international, national, and/or
843 institutional guidelines were followed.
844
845 For electrophysiological experiments in anesthetized rats, unilateral injections of 50-70 nL
846 AAV5-CAG-ArchT-GFP (titer ≥ 7×10^{12} vg/mL; gift from Edward Boyden and purchased
847 through UNC Vector Core; now commercially available from Addgene viral preparation
848 #29777-AAV5; http://n2t.net/addgene:29777; RRID:Addgene_29777) were placed in MT
849 (from interaural zero AP +7.76 to +9.97, ML -1.2, from dura DV -6.6; Paxinos and Watson,
850 2004) or in prelimbic cortical layer 1 (from bregma AP +1.32 mm, ML +0.8 mm with the
851 stereotaxic rotated at a 30° angle towards posterior, from dura DV -3.58 mm with the
852 stereotaxic tilted at a 30° angle; Paxinos and Watson, 2004). Experiments were performed
853 12-16 days after the virus was injected and rats were perfused after the experiment.
854
855 For behavioral experiments that tested the effects of optogenetic inhibition of MT axon
856 terminals in prelimbic cortical layer 1 unilateral injections of 50-70 nL AAV5-CAG-ArchT-
857 GFP (titer ≥ 7×10^{12} vg/mL; gift from Edward Boyden and purchased through UNC Vector
858 Core; now commercially available from Addgene viral preparation #29777-AAV5;
859 http://n2t.net/addgene:29777; RRID:Addgene_29777) or 50-70 nL AAV5-CAG-GFP (titer ≥
860 7×10^{12} vg/mL; gift from Edward Boyden and purchased through UNC Vector Core; now

commercially available from Addgene viral preparation #37825-AAV5; http://n2t.net/addgene:37825; RRID:Addgene_37825) were placed in MT (from interaural zero AP +6.31 to +10.26, ML -1.2, from dura DV -6.6; Paxinos and Watson, 2004). In addition, a LED fiber optic with a diameter of 250 µm and emitting 590 nm (TeleLC-Y-8-250, Bio Research Center Co., Ltd.) was chronically implanted into prelimbic layer 1 (from bregma AP +0.898 mm, ML +1.084 mm with stereotaxic turned at a 30° angle towards posterior, from dura DV -3.58 mm with the stereotaxic tilted at a 30° angle; Paxinos and Watson, 2004) and fixed to the skull with dental cement (Super-Bond C&B, Sun Medical, Japan) in the same aseptic surgery. Behavioral testing was conducted after a recovery period of 12-16 days and rats were perfused after 26-28 days.

For behavioral experiments that tested the effects of chemogenetic inhibition of MT thalamostriatal projections neurons unilateral injections of 50-60 nL AAV5-hSyn-DIO-hM4D(Gi)-mCherry (titer ≥ 7×10^{12} vg/mL; gift from Bryan Roth, Addgene viral preparation #44362-AAV5; http://n2t.net/addgene:44362; RRID: Addgene_44362) or 50-60 nL AAV5-hSyn-DIO-mCherry (titer ≥ 7×10^{12} vg/mL; gift from Bryan Roth, Addgene viral preparation #50459-AAV5; http://n2t.net/addgene:50459; RRID: Addgene_50459) were placed in MT (from interaural zero AP +7.19 to +10.61, ML -1.2, from dura DV -6.6; Paxinos and Watson, 2004). In addition, a second injection of 300 nL AAVrg-pmSyn1-EBFP-Cre (titer: 6×10^{12} vg/mL; gift from Hongkui Zeng; Addgene viral preparation #51507-AAVrg; RRID: Addgene_51507) was placed in striatum (from bregma AP +0.4 mm, ML +3.7 mm, from dura DV -6.1 mm; Paxinos and Watson, 2004) in the same aseptic surgery. Behavioral testing was conducted after a recovery period of 19-25 days and rats were perfused after 28-32 days.

3. In-vivo Electrophysiology

12-16 days after an AAV5-CAG-ArchT-GFP injection had been placed into MT or prelimbic layer 1, rats were anesthetized with 5% isoflurane delivered with room air (1.5-2 L/min, Classic T3 Vaporizer, SurgiVet) and positioned in a stereotaxic frame (custom-build from a Model 1730 Intracellular Frame Assembly from David Kopf Instruments). Anesthesia was maintained at 1.5-2% isoflurane delivered with room air (1.5-2 L/min). An optical fiber with a diameter of 250 µm connected to a 590 nm fiber-coupled LED (ThorLabs, M590F2) that was powered by a high-power, 1-channel LED driver with pulse modulation (ThorLabs, DC2100) was placed in prelimbic layer 1 (from bregma AP +0.898 mm, ML +1.084 mm with stereotaxic turned at a 30° angle towards posterior, from dura DV -3.58 mm with the stereotaxic tilted at a 30° angle)(Paxinos and Watson, 2004). A concentric bipolar platinum/iridium microelectrode with a wire diameter of 25 µm (FHC, CBBPC75) was placed in close proximity to MT (from bregma AP -4.40 mm, ML -1.20 mm, from dura -6.98 mm with the stereotaxic tilted at a 20° angle)(Paxinos and Watson, 2004) and was connected to a biphasic current stimulator (Digitimer, DS4) to stimulate MT and the ascending projections. Both, the 1-channel LED driver and the biphasic current stimulator, were connected to a personal computer by a low-noise data acquisition system (Molecular Devices, Axon CNS Digidata 1440A) that was controlled by Clampex 10.3 to deliver light pulses for optogenetic inhibition and microstimulation using a previously specified protocol. To perform extracellular recordings from neurons in deep layers of prelimbic cortex, glass electrodes with an impedance between 50-110 MΩ were pulled on a P-1000 micropipette puller (Sutter Instrument, P-1000) and placed in prelimbic cortex in lower layer 2/3, layer 4 or layer 5A. Glass electrodes were filled with an internal solution of 3.0 molar potassium methyl sulfate ($KMeSO_4$) that contained goat anti-rat AlexaFluor 594 at a dilution between 1:50 to 1:200, and were coated with 1,1'-dioctadecyl-3,3,3',3'-tetramethylindocarbocyanine

perchlorate stain (DiI stain, 2.5 mg/ml, Thermo Fisher, D282) diluted in one part of ethanol and 9 parts of water. Glass electrodes were connected to a personal computer by a low-noise data acquisition system (Molecular Devices, Axon CNS Digidata 1440A), a Hum Bug Noise Eliminator (Quest Scientific) and a computer-controlled microelectrode amplifier (Molecular Devices, Axon CNS, Axoclamp 900A) and recordings were performed using the Axoclamp 900A software and Clampex 10.3.

Glass electrodes were slowly lowered to the dorsal end of prelimbic cortex in 10 µm steps and then slowly advanced to the ventral end of prelimbic cortex in 0.2-1 µm steps using a micropositioner (David Kopf Instruments, Model 2660). When spiking activity of a neuronal cluster was observed, a protocol was run to stimulate MT and the ascending projections (light OFF trials). For rats, in which AAV5-CAG-ArchT-GFP had been injected into MT, the protocol consisted of 10 sweeps, while for rats that had received AAV5-CAG-ArchT-GFP into prelimbic layer 1, the protocol consisted of 5 sweeps. In both cases, each sweep started with ten 0.5 ms stimulations at -5 mA that were delivered over 1 sec at a rate of 10 Hz followed by a 3-seconds-long pause before the next sweep started. Data was digitized at 250000 Hz. If stimulation of MT and the ascending projections induced spiking activity in a recorded neuronal cluster in prelimbic layers 2/3, 4 or 5A, a second protocol was run. For rats, in which AAV5-CAG-ArchT-GFP had been injected into MT, the protocol was run to determine, whether optogenetic inhibition of MT axon terminals in prelimbic layer 1 reduced spiking activity in the recorded neuronal clusters in prelimbic cortical layers 2/3, 4 or 5A. The protocol consisted of two sweeps. In each sweep the 590 nm light was delivered to prelimbic layer 1 for the first 20 seconds of the sweep (light ON trials). Simultaneously, the protocol featured five iterations of delivering ten 0.5-millisecond-long MT stimulations at -5mA at 10 Hz over a period of 1 second followed by a 3-second-long pause. Twenty seconds

of light delivery were followed by a 4 secs pause before the next sweep started. Data was digitized at 20000 Hz.

For rats that had received AAV5-CAG-ArchT-GFP injections into prelimbic cortical layer 1 instead a second protocol was run to determine, whether activation of archaerhodopsin that induced optogenetic inhibition in layer 1 inhibitory interneurons increased or reduced spiking activity in the recorded neuronal clusters in prelimbic layers 2/3, 4 or 5A. The protocol consisted of three sweeps. In each sweep the 590 nm light was delivered to prelimbic layer 1 for the first 20 seconds of the sweep (light ON trials). Simultaneously, on the first sweep the protocol featured five iterations of delivering ten 0.5-millisecond-long MT stimulations at -5mA at 10 Hz over a period of 1 second followed by a 3-second-long pause. On the second sweep, light delivery was combined with five iterations of delivering ten 0.5-millisecond-long MT stimulations at -3mA at 10 Hz over a period of 1 second followed by a 3-second-long pause. On the third sweep, light delivery was combined with five iterations of delivering ten 0.5-millisecond-long MT stimulations at -1mA at 10 Hz over a period of 1 second followed by a 3-second-long pause. Twenty seconds of light delivery were always followed by a 4-second-long pause before the next sweep started. Data was digitized at 20000 Hz. All data was recorded using a high-band pass filter at 100 Hz and a lowpass Bessel filter at 1 kHz.

4. Perfusion

Rats were anesthetized with approximately 10 ml isoflurane delivered on tissue paper and medetomidine hydrochloride (1.0 mg/kg, intraperitoneal), before being transcardially perfused with either 100 mL 0.1 M phosphate buffer with 2 mg/100 mL heparin (4 °C, pH7.4) or 100 mL of 10% sucrose diluted in Milli-Q, both followed by 150 mL Lana's

fixative (room temperature, 4% depolymerized paraformaldehyde and 14% saturated picric acid solution, Sigma Aldrich, P6744-1GA, in 0.16 M phosphate buffer, pH7.4). Brain tissue was post-fixed for at least 36 h and afterward stored in a 50/50 mixture of Lana's fixative and 20% sucrose in phosphate-buffered saline (PBS) until sectioning, i.e. a minimum of 36 h and up to 2 months.

5. Immunohistochemistry

80 µm-thick coronal or sagittal sections that contained prelimbic cortex (interaural zero +11.52 to +13.68; Paxinos and Watson, 2004), striatum (interaural zero +8.40 to +11.28; Paxinos and Watson, 2004) and/or MT (interaural zero +4.80 to +8.76; Paxinos and Watson, 2004) were taken using a freezing microtome (Yamato, REM-710, Japan). For some sections no immunohistochemistry was performed. These sections were washed in PBS for 4 x 5 min before being mounted. When immunohistochemistry was performed, sections were first washed in PBS for 3 x 5 min. Next, sections were incubated in 20% goat serum (Vector Laboratories, S-1000) or, when the primary antibody was grown in goat, in 20% donkey serum (Millipore, S30-100ML) diluted in PBS, containing 0.05% sodium azide and 0.3% Triton X-100 (Sigma Aldrich, 234729-100ML), at room temperature for 1h. Afterward, sections were incubated for 18h-36h at 4°C in primary antibody solution containing primary antibodies diluted in PBS, 0.05% sodium azide and 0.3% Triton X-100. Then, sections were washed in PBS for 3 x 5 min before being incubated at room temperature for 3h in secondary antibody solution containing secondary antibodies diluted in PBS, 0.05% sodium azide and 0.3% Triton X-100. Finally, sections were washed in PBS for 4 x 5 min. Dilutions of primary and secondary antibodies varied depending on the antibodies used and are provided in table 1. All sections were mounted on glass slides in several drops of mounting medium and sealed with a cover slip. We used UltraCruz Hard-set Mounting Medium with DAPI (Santa Cruz,

sc-359850) or Vectashield HardSet Mounting Medium with DAPI (Vector Laboratories, H-1500) that also provided DNA counterstaining of cell nuclei. If a fluorochrome with an emission spectrum within the blue wavelength was already present within the section, we instead used VectaMount AQ (Vector Laboratories, H-5501). Secondary antibodies were acquired from Millipore or Invitrogen.

Primary antibody	**Secondary antibody**
Mouse anti-GAD67 (Millipore, MAB5406, RRID:AB_2278725): 1:1000 dilution, 0.3% Triton X-100, 18-36h incubation time	Alexa Fluor 594 goat anti-mouse: 1:200 dilution, 3h incubation time
Rabbit anti-GFAP (bioSensis, R-1374, RRID:AB_2492897): 1:1000 dilution, 0.3% Triton X-100, 18-36h incubation time	Alexa Fluor 594 goat anti-rabbit: 1:200 dilution, 3h incubation time
Mouse anti-PV (Sigma, P3088, RRID:AB_477329): 1:1000 dilution, 0.3% Triton X-100, 18h incubation time	Alexa Fluor 488 goat anti-mouse: 1:200 dilution, 3h incubation time
Rabbit anti-bNOS (Sigma, N7280, RRID:AB_260796): 1:500 dilution, 0.3% Triton X-100, 18-36h incubation time	Alexa Fluor 488 goat anti-rabbit: 1:200 dilution, 3h incubation time

Goat anti-CHAT (Millipore, AB144P, RRID:AB_2079751): 1:100 dilution, 0.3% Triton X-100, 18h incubation time	Alexa Fluor 488 donkey anti-goat: 1:200 dilution, 3h incubation time

Table 2. Primary and secondary antibodies used in immunohistochemistry. A summary of dilutions of primary and secondary antibodies in respective antibody solutions, and the dilution of Triton X-100 in primary antibody solutions.

6. Microscopy

Histological verification of the placement of virus injections or LED fiber optics was performed with a fixed stage BX51WI upright microscope from Olympus. A 100W mercury lamp was used as a light source. Alexa Fluor 594 and mCherry were visualized using an excitation filter with a peak at 555 nm and a bandwidth of 25 nm, and an emission filter with a peak at 605 nm and a bandwidth of 25 nm. GFP was visualized using an excitation filter with a peak at 484 nm and a bandwidth of 15 nm, and an emission filter with a peak at 517 nm and a bandwidth of 30 nm. Images were acquired with a 4x objective with a numerical aperture (NA) of 0.16 with the Neurolucida software (MBF Bioscience).

To acquire the high-resolution images presented in this paper, laser confocal scanning microscopy was performed with a Zeiss LSM 780 microscope at room temperature. Images were taken with a 10x objective with a NA of 0.45 or a 63x oil objective with a NA of 1.46 (both objectives from Zeiss). The 63x objective was used with fluorescence-free Immersol immersion oil 518F from Zeiss. Any tiled overview images were acquired with 10% overlap between tiles and stitched using the stitching algorithm provided by the ZEN 2011 SP7 FP1 software (Zeiss, black edition, version 14.0.8.201). An overview of the excitation and

emission peaks of used fluorochromes, the light source and filter set used for excitation, and the emission range used are provided in Table 3.

Fluoro-chrome	**Excitation**	**Emission**	**Light Source**	**Filter Set**	**Emission Range**
DAPI	358 nm	461 nm	405-30 laser diode	MBS 488/561/633 dichroic beam splitter; MBS -405 dichroic beam splitter	410-495 nm
GFP	395 nm	509 nm	Argon laser	MBS 488 dichroic beam splitter	490-590 nm
Alexa Fluor 594	590 nm	617 nm	DPSS 561-10 laser	MBS 458/561 dichroic beam splitter	585-734 nm
mCherry	587 nm	610 nm	DPSS 561-10 laser	MBS 458/561 dichroic beam splitter	578-696 nm

Table 3. Used fluorochromes. Overview of the excitation and emission peak of used fluorochromes, the light source and filter set used for excitation, and the emission range used.

Images were acquired using the ZEN 2011 SP7 FP1 software (Zeiss, black edition, version 14.0.8.201). Brightness and contrast were adjusted using ZEN 2011 SP7 FP1 software (Zeiss, black edition, version 14.0.8.201) and the “Enhance Contrast” option in Fiji (ImageJ version 1.51n or 1.52p). When necessary, brightness and contrast were adjusted separately for each

channel. For final publication, brightness and contrast of images were additionally adjusted using Adobe Photoshop CS5 Extended (version 12.0.4 x64). Adjustments to brightness and contrast were always applied equally across the entire image.

7. Quantification and Statistical Analysis

To quantify and compare decision-making behavior of rats on the three decision-making tasks, we primarily assessed the percentage of trials, in which rats chose 1) the high benefit option on the benefit-benefit decision-making task, 2) the high cost option on the cost-cost-decision-making task or 3) the high cost-high benefit option on the cost-benefit decision-making task out of the total number of non-omitted trials.

In addition, to test whether motor function was disrupted by optogenetic inhibition of MT axon terminals in prelimbic cortical layer 1 or by chemogenetic inhibition of MT striatal-projecting neurons, we assessed 1) the percentage of omitted trials; and 2) the average reaction time across all non-omitted trials.

Behavioral responses in each session were stored in an automatically generated text document. We extracted any variables that were analyzed from these text documents using custom-written Python 3.7 scripts. The reaction times stored in each text document represented a measurement from the presentation of the tone stimulus marking the beginning of each trial to the time rats indicated their choice by pressing one of the two levers. However, reaction times extracted from the text documents were corrected to represent times from presentation of the two levers to the time rats indicated their choice.

To analyze the effect of the injected virus, i.e. ArchT rats as compared to their controls or hM4Di rats as compared to their controls, and the treatment, i.e. light ON versus OFF trials

or D21 agonist versus saline trials, we performed separate ANOVAs for each decision-making task and each variable using the injected virus as between and treatment as within animal variable. When we observed a main or interaction effect, we performed two post-hoc paired t-tests to compare the treatment and non-treatment condition within each group of rats. To confirm that effects were not caused by pre-existing differences in behavior between the two groups of rats, we further performed two Student's t-tests to compare behavior on the first 20 trials of the last day of training as well as behavior in the non-treatment condition between the two groups of rats. To confirm that effects were not caused by surgery, we also compared the behavior pre- and post-surgery within each group of rats. We usually performed 6 t-tests to analyze each behavioral variable. We applied a Bonferroni correction to the significance level resulting in a significance level of $p=0.0083$. However, when comparing the effect of optogenetic inhibition of MT axon terminals in prelimbic cortical layer 1 on choice behavior, we also compared differences in choice behavior between light ON and OFF trials for each individual day of behavioral testing. In addition, we compared differences in the percentage of high benefit and high cost choices between the first and last 20 trials on the last three days of behavioral training. Overall, the number of statistical tests resulted in an adjusted significance level of $p=0.0028$.

We observed a significant difference in the percentage of high cost-high benefit choices between light ON and OFF trials for ArchT rats. To quantify the size of the difference, we subtracted the percentage in light OFF from that in light ON trials. We performed a Student’s t-test on this new metric (significance level of $p=0.05$), comparing it between controls and ArchT rats, to analyze whether the difference in the percentage of high cost-high benefit trials was significantly different between the two groups of rats.

We adjusted individual dilutions of sweetened condensed milk for each animal, so that each animal would choose the high cost-high benefit option as well as the low cost-low benefit option in about 50% of non-omitted trials. We used the first 3 days of behavioral training on the cost-benefit decision-making task to adjust individual dilutions. We systematically varied the dilution of sweetened condensed milk on every 20 trials. Hence, data on the percentage of high cost-high benefit choices, which was collected across these 3 days, does not represent the actual choice behavior of rats on days after we determined and used their individual dilutions. Only a few rats did not reach criterion on the cost-benefit decision-making task within the first 3 days, resulting in few rats being trained for additional days. When running statistical tests that involved data from the last day of behavioral training on the cost-benefit decision-making task, we only used the data from the first 20 trials on the last day of behavioral training for these few rats. For all other rats, when the determined individual dilution corresponded to a dilution that was used during the adjustment process, we used data from those 20 trials. Otherwise, when the individual dilution was between dilutions used during the adjustment process, we averaged data from the 20 trials with the next higher and the 20 trials with the next lower dilution. Given the limitations of this approach, we compared a second metric between groups of rats to determine whether pseudo-random assignment of rats to either the control or ArchT group influenced the percentage of high cost-high benefit choices within each group. We analyzed for each group of rats whether the individual dilution of sweetened condensed milk correlated with the percentage of high cost-high benefit choices in light OFF trials during behavioral testing. We assumed that if these two metrics did not correlate, pseudo-random assignment of rats would not have influenced the percentage of high cost-high benefit choices in each group, even if the determined individual dilutions of sweetened condensed milk would have varied vastly. We calculated Kendall's Tau to determine the correlation between the two metrics. We chose Kendall's Tau since

individual dilutions of sweetened condensed milk were rounded to the closest whole number and, hence, on an ordinal scale. We chose Kendall's Tau over Spearman's rho due to the small sample size and higher robustness of Kendall's Tau for small sample sizes.

Statistical analyses were performed in R (version 3.6.3). We tested the assumption of the data being normal distributed, which is a prerequisite for parametric tests, with Levene's test and the assumption of homogeneity of variances with Shapiro's test.

We used custom-written Matlab scripts (Matlab 2019b) to analyze electrophysiological data collected in anesthetized rats. Data were filtered at 100 Hz to 10 kHz at the time of recordings and no further filtering was done. To analyze the effect of optogenetic inhibition of MT axon terminals or inhibitory interneurons in prelimbic cortical layer 1 on neuronal cluster responses recorded in deep layers of prelimbic cortex, we defined segments starting 20 ms before and ending 80 ms after MT stimulations were delivered. We normalized each data segment by subtracting the average activity measured across the last 40 ms of each segment from each data point in the segment. MT stimulations induced an artefact, which was truncated from any presented figures by removing data from the time of MT stimulation until 2 ms after. For each cell, the threshold to identify extracellular spikes was determined by using the Matlab 'findpeaks'-algorithm with a minimum spike prominence of 0.5 mV on data segments from light OFF trials. We identified the spike with the largest spike prominence and identified extracellular spikes by running the 'findpeaks'-algorithm again, but using 30% of the largest identified spike prominence as minimum spike prominence. We constructed a peri-stimulus time histogram with a bin width of 0.1 ms from the data. To compare the average number of spikes per millisecond between light ON and OFF trials

within the first 20 ms after MT stimulation, we conducted a Wilcoxon ranked-sign test across cells.

To compare the width of spikes during segments of spontaneous activity, after MT stimulation in light OFF trials and after MT stimulation in light ON trials, we analyzed the last 2 seconds of each light OFF sweep. Each light OFF sweep started with ten MT stimulations followed by a 3-second-long pause before the next sweep started. Spontaneous activity was observed within this 3-second-long pause of which we analyzed the last 2 seconds. Data within these 2-second-long segments were normalized by subtracting the average activity measured across the last 40 ms of each segment from each data point in the segment. The width of spikes within these segments of spontaneous activity, for light OFF and for light ON trials were identified by running the Matlab 'findpeaks'-algorithm and using the previously determined value for minimum spike prominence. Spike widths were summarized in histograms. In addition, segments showing activity after MT stimulation in light OFF trials as well as spontaneous activity were plotted for selected cells.

To test whether rebound spiking was observed upon turning the 590 nm light off, which deactivated the archaerhodopsin and terminated optogenetic inhibition of MT axon terminals, we extracted segments from light ON trials starting 100 ms before and ending 100 ms after the light was turned off. Data was normalized by subtracting the mean activity across each segment from each data point in the segment. We again identified extracellular spikes by running the Matlab 'findpeaks'-algorithm and using the previously determined value for minimum spike prominence. We constructed a peri-stimulus time histogram from the data using a bin size of 1 ms. In addition, the average number of spikes per second for the 100 ms

1147 before and the 100 ms after the light was turned off was calculated and indicated in the peri-
1148 stimulus time histogram by a red dotted line.

1149

1150 *8. Data Availability*

1151 Raw behavioral data, raw electrophysiology data and analysis scripts used to generate figure
1152 1 through 4 are available on Github (https://github.com/bsieveri/sieveritz-2022-mt-
1153 prelimbic). Microscopy data will be made available upon request.

1154

1155 **Appendix 1**

		Training						Testing					
		Day -3		Day -2		Day -1		Day 1		Day 2		Day 3	
		p-value	r (effect size)	p-value	r (effect size)	p-value	r (effect size)	p-value	r (effect size)	p-value	r (effect size)	p-value	r (effect size)
Benefit-Benefit Decision-Making	Change in High Benefit Choices (%), Controls	0.097	0.48	0.013	0.668	0.061	0.533	0.039	0.575	0.028	0.606	0.156	0.418
	Change in High Benefit Choices (%), ArchT Rats	0.007	0.757	0.156	0.459	0.002	0.821	0.179	0.437	0.073	0.561	0.113	0.505
Cost-Cost Decision-Making	Change in High Cost Choices (%), Controls	0.186	0.391	0.013	0.665	0.009	0.692	0.081	0.501	0.041	0.572	0.702	0.12
	Change in High Cost Choices (%), ArchT Rats	0.019	0.687	0.24	0.387	0.211	0.409	0.083	0.545	0.033	0.642	0.463	0.248
Cost-Benefit Decision-Making	Change in High Cost-High Benefit Choices (%), Controls	N/A	N/A	N/A	N/A	0.306	0.455	0.678	0.127	0.717	0.111	0.768	0.091
	Change in High Cost-High Benefit Choices (%), ArchT Rats	N/A	N/A	N/A	N/A	0.282	0.602	0.012	0.725	0.0037	0.791	0.041	0.623

Appendix 1 - Table 1. Overview of p-values and effect sizes for t-tests comparing choice behavior on each individual behavioral testing days and on the last three days of behavioral training. The percentage of high benefit, high cost or high cost-high benefit choices within each group of rats was compared between light ON and OFF trials for each individual day of behavioral testing, or between the first and last 20 trials on the last three days of behavioral training. Training day -1 indicates the last day of behavioral training, training day -2 the second to last day and training day -3 the day prior to the second to last day. To account for multiple comparisons, t-tests were conducted using a Bonferroni corrected significance level of p=0.0028.

		High cost-high benefit/high benefit/high cost choices (%)		Omitted Trials (%)		Overall Reaction Time	
		p-value	r (effect size)	p-value	r (effect size)	p-value	r (effect size)
Benefit-Benefit Decision-Making	ArchT Rats versus Controls, Pre-Surgery	0.231	0.271	0.113	0.372	0.178	0.301
	ArchT Rats versus Controls, Post-Surgery	0.493	0.161	0.444	0.195	0.189	0.294
	Pre- versus Post-surgery, Controls	0.07	0.518	0.097	0.479	0.009	0.693
	Pre- versus Post-surgery, ArchT Rats	0.011	0.505	0.437	0.262	0.017	0.698
Cost-Cost Decision-Making	ArchT Rats versus Controls, Pre-Surgery	0.243	0.282	0.25	0.256	0.132	0.333
	ArchT Rats versus Controls, Post-Surgery	0.768	0.069	0.668	0.111	0.065	0.432
	Pre- versus Post-surgery, Controls	0.043	0.569	0.019	0.637	0.047	0.56
	Pre- versus Post-surgery, ArchT Rats	0.006	0.768	0.91	0.039	0.04	0.625
Cost-Benefit Decision-Making	ArchT Rats versus Controls, Pre-Surgery	0.463	0.172	0.261	0.26	0.403	0.2
	ArchT Rats versus Controls, Post-Surgery	0.444	0.178	0.601	0.153	0.509	0.153

	Pre- versus Post-surgery, Controls	0.589	0.165	0.731	0.106	0.063	0.53
	Pre- versus Post-surgery, ArchT Rats	0.667	0.147	0.356	0.308	0.076	0.556
Bonferroni corrected significance level:		p=0.0028		p=0.0083		p=0.0083	

Appendix 1 - Table 2. Overview of p-values and effect sizes for post hoc t-tests comparing the choice behavior, percentage of omitted trials and reaction times on non-omitted trials between ArchT rats and their controls as well as within each group pre- and post-surgery. Bonferroni-corrected significance levels for each metric are indicated in the bottom row.

Competing Interests

We declare no competing interests.

Author Contributions

Conceptualization, B.S. and G.W.A.; Methodology, B.S., J.R.W. and G.W.A.; Software, B.S.; Formal Analysis, B.S.; Investigation, B.S. and S.H.D.; Writing – Original Draft, B.S., S.H.D., J.R.W. and G.W.A.; Visualization, B.S.; Supervision, J.R.W. and G.W.A.

References

Amemori KI, Amemori S, Gibson DJ, Graybiel AM. 2020. Striatal Beta Oscillation and Neuronal Activity in the Primate Caudate Nucleus Differentially Represent Valence and Arousal Under Approach-Avoidance Conflict. *Front Neurosci* **14**:1–17. doi:10.3389/fnins.2020.00089

Amemori KI, Graybiel AM. 2012. Localized microstimulation of primate pregenual cingulate cortex induces negative decision-making. *Nat Neurosci* **15**:776–785. doi:10.1038/nn.3088

1187 Arbuthnott GW, MacLeod NK, Maxwell DJ, Wright AK. 1990. Distribution and synaptic
1188 contacts of the cortical terminals arising from neurons in the rat ventromedial thalamic
1189 nucleus. *Neuroscience* **38**:47–60. doi:10.1016/0306-4522(90)90373-C
1190 Augur IF, Wyckoff AR, Aston-Jones G, Kalivas PW, Peters J. 2016. Chemogenetic
1191 activation of an extinction neural circuit reduces cue-induced reinstatement of cocaine
1192 seeking. *J Neurosci* **36**:10174–10180. doi:10.1523/JNEUROSCI.0773-16.2016
1193 Aupperle RL, Paulus MP. 2010. Neural systems underlying approach and avoidance in
1194 anxiety disorders. *Dialogues Clin Neurosci* **12**:517–31.
1195 Brazhnik E, McCoy AJ, Novikov N, Hatch CE, Walters JR. 2016. Ventral Medial Thalamic
1196 Nucleus Promotes Synchronization of Increased High Beta Oscillatory Activity in the
1197 Basal Ganglia-Thalamocortical Network of the Hemiparkinsonian Rat. *J Neurosci*
1198 **36**:4196–4208. doi:10.1523/JNEUROSCI.3582-15.2016
1199 Brecht M, Sakmann B. 2002. Whisker maps of neuronal subclasses of the rat ventral
1200 posterior medial thalamus, identified by whole-cell voltage recording and morphological
1201 reconstruction. *J Physiol* **538**:495–515. doi:10.1113/jphysiol.2001.012334
1202 Catanese J, Jaeger D. 2021. Premotor ramping of thalamic neuronal activity is modulated by
1203 nigral inputs and contributes to control the timing of action release. *J Neurosci* **41**:1878–
1204 1891. doi:10.1523/JNEUROSCI.1204-20.2020
1205 Collins DP, Anastasiades PG, Marlin JJ, Carter AG. 2018. Reciprocal Circuits Linking the
1206 Prefrontal Cortex with Dorsal and Ventral Thalamic Nuclei. *Neuron* **98**:366-379.e4.
1207 doi:10.1016/j.neuron.2018.03.024
1208 Cruikshank SJ, Ahmed OJ, Stevens TR, Patrick SL, Gonzalez AN, Elmaleh M, Connors BW.
1209 2012. Thalamic Control of Layer 1 Circuits in Prefrontal Cortex. *J Neurosci* **32**:17813–
1210 17823. doi:10.1523/JNEUROSCI.3231-12.2012
1211 De La Peña E, Geijo-Barrientos E. 2000. Participation of low-threshold calcium spikes in

excitatory synaptic transmission in guinea pig medial frontal cortex. *Eur J Neurosci* **12**:1679–1686. doi:10.1046/j.1460-9568.2000.00061.x

Deisseroth K. 2021. Predicted irradiance values: model based on direct measurements in mammalian brain tissue. https://web.stanford.edu/group/dlab/cgi-bin/graph/chart.php

Elena Erro M, Lanciego JL, Giménez-Amaya JM. 2002. Re-examination of the thalamostriatal projections in the rat with retrograde tracers. *Neurosci Res* **42**:45–55. doi:10.1016/S0168-0102(01)00302-9

Floresco SB, Grace AA. 2003. Gating of hippocampal-evoked activity in prefrontal cortical neurons by inputs from the mediodorsal thalamus and ventral tegmental area. *J Neurosci* **23**:3930–43.

Friedman A, Homma D, Bloem B, Gibb LG, Amemori K ichi, Hu D, Delcasso S, Truong TF, Yang J, Hood AS, Mikofalvy KA, Beck DW, Nguyen N, Nelson ED, Toro Arana SE, Vorder Bruegge RH, Goosens KA, Graybiel AM. 2017. Chronic Stress Alters Striosome-Circuit Dynamics, Leading to Aberrant Decision-Making. *Cell* **171**:1191-1205.e28. doi:10.1016/j.cell.2017.10.017

Friedman A, Homma D, Gibb LG, Amemori KI, Rubin SJ, Hood AS, Riad MH, Graybiel AM. 2015. A corticostriatal path targeting striosomes controls decision-making under conflict. *Cell* **161**:1320–1333. doi:10.1016/j.cell.2015.04.049

Gaidica M, Hurst A, Cyr C, Leventhal DK. 2018. Distinct Populations of Motor Thalamic Neurons Encode Action Initiation, Action Selection, and Movement Vigor. *J Neurosci* **38**:6563–6573. doi:10.1523/JNEUROSCI.0463-18.2018

Guo Z V., Inagaki HK, Daie K, Druckmann S, Gerfen CR, Svoboda K. 2017. Maintenance of persistent activity in a frontal thalamocortical loop. *Nature* **545**:181–186. doi:10.1038/nature22324

Herkenham M. 1979. The afferent and efferent connections of the ventromedial thalamic

nucleus in the rat. *J Comp Neurol* **183**:487–517. doi:10.1002/cne.901830304

Hosking JG, Cocker PJ, Winstanley CA. 2014. Dissociable contributions of anterior cingulate cortex and basolateral amygdala on a rodent cost/benefit decision-making task of cognitive effort. *Neuropsychopharmacology* **39**:1558–1567. doi:10.1038/npp.2014.27

Ironside M, Amemori K ichi, McGrath CL, Pedersen ML, Kang MS, Amemori S, Frank MJ, Graybiel AM, Pizzagalli DA. 2020. Approach-Avoidance Conflict in Major Depressive Disorder: Congruent Neural Findings in Humans and Nonhuman Primates. *Biol Psychiatry* **87**:399–408. doi:10.1016/j.biopsych.2019.08.022

Jiang X, Wang G, Lee AJ, Stornetta RL, Zhu JJ. 2013. The organization of two new cortical interneuronal circuits. *Nat Neurosci* **16**:210–218. doi:10.1038/nn.3305

Johansson Y, Silberberg G. 2020. The Functional Organization of Cortical and Thalamic Inputs onto Five Types of Striatal Neurons Is Determined by Source and Target Cell Identities. *Cell Rep* **30**:1178-1194.e3. doi:10.1016/j.celrep.2019.12.095

Klug JR, Engelhardt MD, Cadman CN, Li H, Smith JB, Ayala S, Williams EW, Hoffman H, Jin X. 2018. Differential inputs to striatal cholinergic and parvalbumin interneurons imply functional distinctions. *Elife* **7**:e35657. doi:10.7554/eLife.35657

Kubota Y. 2014. Untangling GABAergic wiring in the cortical microcircuit. *Curr Opin Neurobiol* **26**:7–14. doi:10.1016/j.conb.2013.10.003

Kuramoto E, Furuta T, Nakamura KC, Unzai T, Hioki H, Kaneko T. 2009. Two types of thalamocortical projections from the motor thalamic nuclei of the rat: A single neuron-tracing study using viral vectors. *Cereb Cortex* **19**:2065–2077. doi:10.1093/cercor/bhn231

Lapper SR, Bolam JP. 1992. Input from the frontal cortex and the parafascicular nucleus to cholinergic interneurons in the dorsal striatum of the rat. *Neuroscience* **51**:533–545. doi:10.1016/0306-4522(92)90293-B

1262 Lee AJ, Wang G, Jiang X, Johnson SM, Hoang ET, Lanté F, Stornetta RL, Beenhakker MP,
1263 Shen Y, Julius Zhu J. 2015. Canonical Organization of Layer 1 Neuron-Led Cortical
1264 Inhibitory and Disinhibitory Interneuronal Circuits. *Cereb Cortex* **25**:2114–2126.
1265 doi:10.1093/cercor/bhu020
1266 Loewke AC, Minerva AR, Nelson AB, Kreitzer AC, Gunaydin LA. 2021. Frontostriatal
1267 Projections Regulate Innate Avoidance Behavior. *J Neurosci* **41**:5487–5501.
1268 doi:10.1523/JNEUROSCI.2581-20.2021
1269 Mahn M, Prigge M, Ron S, Levy R, Yizhar O. 2016. Biophysical constraints of optogenetic
1270 inhibition at presynaptic terminals. *Nat Neurosci* **19**:554–6. doi:10.1038/nn.4266
1271 Martin-Cortecero J, Nuñez A. 2016. Sensory responses in the medial prefrontal cortex of
1272 anesthetized rats. Implications for sensory processing. *Neuroscience* **339**:109–123.
1273 doi:10.1016/j.neuroscience.2016.09.045
1274 Matsuyama K, Tanaka M. 2021. Temporal prediction signals for periodic sensory events in
1275 the primate central thalamus. *J Neurosci* **41**:1917–1927. doi:10.1523/jneurosci.2151-
1276 20.2021
1277 Mobini S, Body S, Ho MY, Bradshaw C, Szabadi E, Deakin J, Anderson I. 2002. Effects of
1278 lesions of the orbitofrontal cortex on sensitivity to delayed and probabilistic
1279 reinforcement. *Psychopharmacology (Berl)* **160**:290–298. doi:10.1007/s00213-001-
1280 0983-0
1281 Nakano Y, Karube F, Hirai Y, Kobayashi K, Hioki H, Okamoto S, Kameda H, Fujiyama F.
1282 2018. Parvalbumin-producing striatal interneurons receive excitatory inputs onto
1283 proximal dendrites from the motor thalamus in male mice. *J Neurosci Res* **96**:1186–
1284 1207. doi:10.1002/jnr.24214
1285 Ozawa T, Ycu EA, Kumar A, Yeh LF, Ahmed T, Koivumaa J, Johansen JP. 2017. A
1286 feedback neural circuit for calibrating aversive memory strength. *Nat Neurosci* **20**:90–

97. doi:10.1038/nn.4439

Paxinos G, Watson C. 2004. The Rat Brain in Stereotaxic Coordinates - The New Coronal Set 5th Edition. Cambridge: Academic Press. doi:10.1016/0143-4179(83)90049-5

Peirce JW. 2007. PsychoPy-Psychophysics software in Python. *J Neurosci Methods* **162**:8–13. doi:10.1016/j.jneumeth.2006.11.017

Pockberger H. 1991. Electrophysiological and morphological properties of rat motor cortex neurons in vivo. *Brain Res* **539**:181–190. doi:10.1016/0006-8993(91)91619-C

Saalmann YB, Kastner S. 2011. Cognitive and Perceptual Functions of the Visual Thalamus. *Neuron* **71**:209–223. doi:10.1016/j.neuron.2011.06.027

Schwabe L, Wolf OT. 2009. Stress prompts habit behavior in humans. *J Neurosci* **29**:7191–8. doi:10.1523/JNEUROSCI.0979-09.2009

Sidibé M, Smith Y. 1999. Thalamic inputs to striatal interneurons in monkeys: Synaptic organization and co-localization of calcium binding proteins. *Neuroscience* **89**:1189–1208. doi:10.1016/S0306-4522(98)00367-4

Sieveritz B, Arbuthnott GW. 2020. Prelimbic cortical targets of ventromedial thalamic projections include inhibitory interneurons and corticostriatal pyramidal neurons in the rat. *Brain Struct Funct* **225**:2057–2076. doi:10.1007/s00429-020-02109-3

Smith Y, Raju D V., Pare JF, Sidibe M. 2004. The thalamostriatal system: A highly specific network of the basal ganglia circuitry. *Trends Neurosci*. doi:10.1016/j.tins.2004.07.004

Sousa N, Almeida OFX. 2012. Disconnection and reconnection: The morphological basis of (mal)adaptation to stress. *Trends Neurosci* **35**:742–751. doi:10.1016/j.tins.2012.08.006

Stafstrom CE, Schwindt PC, Chubb MC, Crill WE. 1985. Properties of persistent sodium conductance and calcium conductance of layer V neurons from cat sensorimotor cortex in vitro. *J Neurophysiol* **53**:153–170. doi:10.1152/jn.1985.53.1.153

Stefanik MT, Kalivas PW. 2013. Optogenetic dissection of basolateral amygdala projections

during cue-induced reinstatement of cocaine seeking. *Front Behav Neurosci* **7**:1–6. doi:10.3389/fnbeh.2013.00213

Stefanik MT, Kupchik YM, Brown RM, Kalivas PW. 2013a. Optogenetic evidence that pallidal projections, not nigral projections, from the nucleus accumbens core are necessary for reinstating cocaine seeking. *J Neurosci* **33**:13654–13662. doi:10.1523/JNEUROSCI.1570-13.2013

Stefanik MT, Kupchik YM, Kalivas PW. 2016. Optogenetic inhibition of cortical afferents in the nucleus accumbens simultaneously prevents cue-induced transient synaptic potentiation and cocaine-seeking behavior. *Brain Struct Funct* **221**:1681–1689. doi:10.1007/s00429-015-0997-8

Stefanik MT, Moussawi K, Kupchik YM, Smith KC, Miller RL, Huff ML, Deisseroth K, Kalivas PW, Lalumiere RT. 2013b. Optogenetic inhibition of cocaine seeking in rats. *Addict Biol* **18**:50–53. doi:10.1111/j.1369-1600.2012.00479.x

Stujenske JM, Spellman T, Gordon JA. 2015. Modeling the Spatiotemporal Dynamics of Light and Heat Propagation for InVivo Optogenetics. *Cell Rep* **12**:525–534. doi:10.1016/j.celrep.2015.06.036

Tepper JM, Koós T, Ibanez-Sandoval O, Tecuapetla F, Faust TW, Assous M. 2018. Heterogeneity and diversity of striatal GABAergic interneurons: Update 2018. *Front Neuroanat* **12**:1–14. doi:10.3389/fnana.2018.00091

Walton ME, Bannerman DM, Alterescu K, Rushworth MFS. 2003. Functional specialization within medial frontal cortex of the anterior cingulate for evaluating effort-related decisions. *J Neurosci* **23**:6475–9. doi:23/16/6475 [pii]

Williams LE, Holtmaat A. 2019. Higher-Order Thalamocortical Inputs Gate Synaptic Long-Term Potentiation via Disinhibition. *Neuron* **101**:91-102.e4. doi:10.1016/j.neuron.2018.10.049

1337 Wolff M, Morceau S, Folkard R, Martin-Cortecero J, Groh A. 2021. A thalamic bridge from
1338 sensory perception to cognition. *Neurosci Biobehav Rev* **120**:222–235.
1339 doi:10.1016/j.neubiorev.2020.11.013
1340 Yuan B, Morrow TJ, Casey KL. 1985. Responsiveness of ventrobasal thalamic neurons after
1341 suppression of S1 cortex in the anesthetized rat. *J Neurosci* **5**:2971–2978.
1342 doi:10.1523/jneurosci.05-11-02971.1985
1343